Measurement of Nonlinear Normal Modes using Multi-Harmonic Stepped Force Appropriation and Free Decay

David A. Ehrhardt

Graduate Research Assistant, Ph.D. Candidate

dehrhardt@wisc.edu

&

Matthew S. Allen

Associate Professor

msallen@engr.wisc.edu

Department of Engineering Physics

University of Wisconsin-Madison

534 Engineering Research Building

1500 Engineering Drive

Madison, WI 53706

Abstract

Nonlinear Normal Modes (NNMs) offer tremendous insight into the dynamic behavior of a nonlinear system, extending many concepts that are familiar in linear modal analysis. Hence there is interest in developing methods to experimentally and numerically determine a system's NNMs for model updating or simply to characterize its dynamic response. Previous experimental work has shown that a mono-harmonic excitation can be used to isolate a system's dynamic response in the neighborhood of a NNM along the main backbones of a system. This work shows that a multi-harmonic excitation is needed to isolate a NNM when well separated linear modes of a structure couple to produce an internal resonance. It is shown that one can tune the multiple harmonics of the input excitation using a plot of the input force versus the response velocity until the area enclosed by the force-velocity curve is minimized. Once an appropriated NNM is measured, one can increase the force level and retune the frequency to obtain a NNM at a higher amplitude or remove the excitation and measure the structure's decay down a NNM backbone. This work explores both methods using simulations and measurements of a nominally-flat clamped-clamped beam excited at a single point with a magnetic force. Numerical simulations are used to validate the method in a well defined environment and to provide comparison with the experimentally measured NNMs. The experimental results seem to produce a good estimate of two NNMs along their backbone and part of an internal resonance branch. Full-field measurements are then used to further explore the couplings between the underlying linear modes along the identified NNMs.

Keywords: Nonlinear Normal Mode, Experimental Force Appropriation, Continuous-Scan Laser Doppler Vibrometry,

1 Introduction

Over the past several decades a suite of testing and modeling techniques has been developed to quantify the dynamic motion of a structure using its linear modal properties (e.g. resonant frequencies, mode shapes, and damping ratios) [1-3]. The measured or calculated modal properties are typically used to quantify the inertial (mass), elastic (stiffness), and dissipation (damping) characteristics of a structure. Modal properties provide the benefit of describing the global dynamics of a structure using a small number of parameters, and can also be used to predict the response due to an arbitrary excitation thanks to invariance, superposition, etc... The classical (undamped) Linear Normal Modes (LNMs), that are of interest to this work, can be considered a special case of *Complex Modes*; LNMs are directly related to resonant responses of a structure only when dissipation is well approximated as proportional to the mass and stiffness matrices [4]. LNMs are particularly useful in decoupling the equations of motion, allowing one to find the response of the structure through a summation of individual single degree of freedom responses. Further details can be found in many textbooks [5-8].

When a structure exhibits the nonlinear force-displacement relationships that are typical of geometrically nonlinear structures under large amplitude loading conditions, the dynamic response characteristics change with amplitude. For large response amplitudes, LNMs no longer uncouple the undamped equations of motion [9] and so the dynamic motion can no longer be thought of as a summation of uncoupled single degree of freedom systems. An alternate definition of modes has been sought, presumably with the hope that an extended superposition principle could be developed and used to solve the nonlinear equations of motion. While that has proved elusive – superposition does not hold for any of the existing definitions of NNMs – these definitions have led to considerable insight into the dynamics of complicated systems and thus proven useful for engineers [11, 12]. Rosenberg [10] was the first to pursue a definition, coining the name *Nonlinear Normal Modes* (NNMs) to describe certain *synchronous oscillations* exhibited by the conservative nonlinear equations of motion. This definition was subsequently

simplified and expanded to include internal resonances by defining a NNM as simply a *not necessarily synchronous periodic oscillation* of the conservative nonlinear equations of motion [10]. Some NNMs described using this definition originate from a structure's LNMs at low response amplitudes, but NNMs can also describe jumps, bifurcations, internal resonances, modal interactions and sub- and super-harmonic responses which have no counterpart in linear systems [11, 12]. Much of the initial work on NNMs to date has focused on analytical or numerical investigations of low-order lumped-mass systems or Galerkin models of simple continua [10-18]. Recently, methods have been developed which extend the numerical calculation of NNMs to more complicated structures which are described by geometrically nonlinear finite element models (FEMs) [19, 20].

While NNMs are a new concept, they have found some use already in several applications. For example, NNMs have been used to provide insights to guide the design of nonlinear vibration absorbers [21]. With the extension mentioned above and in [19, 20], they are now also being used to characterize FE models of complicated, geometrically nonlinear structures. For example, they were used to correlate simulations [22] with experimental measurements [23, 24] and to assess the fidelity of simulation models [20]. The insights that they provide could also be used to guide the design of a nonlinear structure in general or to evaluate advanced model reduction techniques.

This work focuses on an extension of experimental modal analysis (EMA) techniques in which a harmonic forcing is used to experimentally isolate NNMs [22]. EMA methodologies can be broadly split into two areas classified by the number of LNMs measured during a test. Phase Separation Methods (PSMs) excite multiple LNMs at a time with broadband excitation and then the response is decomposed using modal parameter estimation techniques to identify the LNMs that are active in the response. These are the most popular and commonly used methods for linear experimental modal parameter identification. Several works have sought to extend these to nonlinear identification, [9, 25, 26], but in the presence of nonlinearity the response is not a simple superposition of LNMs, and indeed one may not even be able to accurately postulate the form of the mathematical model a priori, so this becomes challenging. Furthermore, as these methods are applied to higher order systems the number of terms to be identified can become excessive.

Phase Resonance Methods (PRMs) excite one LNM at a time by tuning the input force and monitoring the phase of the response until a criterion is met and the measured response becomes the LNM of interest. They are less popular in linear EMA because they can be time-consuming. However, PRMs are still used in Ground Vibration Tests where closely spaced modes occur and highly accurate results (especially in regards to damping) are needed. [27-29]. For linear systems, several methods have been developed [30-33] to identify the distribution of the input force needed to cause the response to lag the input force by 90 degrees, thus fulfilling the phase lag criterion. In the presence of nonlinearity, linear PRMs have still been applied and when the classical phase condition is met, they are thought to provide a quasi-linearization of the nonlinear structure that can be used to access the dependency of resonant frequencies, structural damping, and generalized mass with the amplitude of structural responses [29]. PRMs have also begun to be extended to the measurement of NNMs through the implementation of different methods of force appropriation. For instance, a method called force appropriation of nonlinear systems (FANS) was presented in [34] that uses a multi-point, multi-harmonic force to isolate a single LNM in nonlinear response regimes. This is done by iteratively canceling any coupling between LNMs. Then one can identify the nonlinear characteristics of the isolated mode without modal coupling terms. This work follows a different approach, pioneered by Peeters et al. who presented a rigorous theory by which an undamped NNM could be isolated in a measurement [22, 23]. They showed that a multi-point multi-harmonic sine wave could cancel damping and isolate a general NNM. It was then demonstrated both analytically and experimentally that a single-point single harmonic force could be used to isolate a response in the neighborhood of a single NNM

with good accuracy [23, 24]. In these investigations, once phase lag quadrature was met, the input force was turned off and the response allowed to decay tracing the backbone of the NNM.

This work explores a means whereby multi-harmonic excitation (i.e. a signal containing a fundamental frequency, ω, and various integer harmonics, 2ω, 3ω, 4ω, etc…) can be used to isolate a NNM. The theory shows that a simple metric based on a plot of the input force versus response velocity can be used to monitor the phase condition in real time, and to understand which harmonics should be added to the input force to minimize the phase condition. The results also show that the phases of the response and its harmonics are highly sensitive to perturbations and so the mode indicator function appears to be a more useful metric in gauging whether an adequate estimate of the NNM has been obtained. The methods are tested by measuring two NNMs of a flat clamped-clamped beam. Modal interactions from internal resonances are detected experimentally and isolated to the level permitted with the current setup.

The next section briefly reviews the theory underlying NNMs using the simulated NNMs from a finite element model (FEM) of the structure of interest to illustrate key concepts. Then the force appropriation methodology is reviewed as well as the proposed extensions that facilitate the tuning of multi-harmonic excitation signals that is applied in simulation. The experimental setup and results are then described in Section 3.

2 Theory

2.1 Nonlinear Normal Modes

2.1.1 Introduction

Similar to the LNMs reviewed in the appendix, the definition of NNMs used in this work is rooted in the conservative nonlinear free vibration EOM:

$$\mathbf{M}\ddot{\mathbf{x}}(t) + \mathbf{f}_{\mathbf{nl}}(\mathbf{x}, \mathbf{x}:\mathbf{x}, \mathbf{x}:\mathbf{x}:\mathbf{x}) = 0 \tag{1}$$

where $\mathbf{f}_{\mathbf{nl}}$ is the nonlinear restoring force which is purely a function of displacement (e.g. including only stiffness terms). The nonlinear restoring force can be represented by many functional forms depending on the type of nonlinearity expected (e.g. polynomial stiffness and damping, clearances, impacts, friction, and saturation effects). This work focuses on pure geometric nonlinearities, in which case the restoring force is a nonlinear function of displacement, typically expressed as a polynomial with second order terms that typically corresponds to a spring softening effect, or a decrease in the fundamental frequency of vibration for increasing energy levels, and third order polynomial terms that typically correspond to a spring hardening. The clamped-clamped flat beam examined in this work exhibits these physics due to coupling between bending and axial stretching, see [35, 36] for a more thorough treatment.

2.1.2 Example: Numerically Computed NNMs of the Flat Beam

A 41-node finite element model (FEM) was created for the flat clamped-clamped beam whose dimensions are given in Sec. 3.1. The finite element model used here is identical to that described in [18]. A few methods were recently developed to calculate the NNMs [18, 20] of a finite element models such as this; the numerical results presented here were calculated using the applied modal force numerical continuation technique [18], which iterates on the nonlinear transient response of the FEM until a periodic solution is obtained. Hence, the NNMs that it calculates satisfy the geometrically nonlinear FEM to some tolerance.

For convenience, 'families' of NNMs can be presented in frequency-energy plots (FEPs) based on the fundamental frequency of the response and total energy conserved over a period of the response. Three distinct 'families' of NNMs of the flat beam will be discussed in this investigation. The first 'family' corresponds to the nonlinear continuation of LNM-1, also called

the backbone of NNM-1, which is shown in Fig. 1(a) in blue. The flat beam exhibits a spring hardening nonlinearity, or an increase in the fundamental frequency of vibration with increased input energy as discussed in [36, 37]. A change in the fundamental frequency of vibration of 36% is captured along this backbone. For reference, a demarcation is added to these plots showing the energy at which the maximum displacement amplitude would be equal to one beam thickness (i.e. 0.76mm). The second 'family' corresponds to a 5:1 harmonic coupling between LNM-1 and LNM3, or an internally resonant bifurcation from NNM-1 and is shown in Fig. 1a in red.

To illustrate the deformation of the beam at various points on the frequency energy plot, the deformation of the beam throughout a quarter period of the response is shown in Figs. 1(b)-(e) and the Fourier coefficients of the response are shown in Figs. 1(f)-(i) Figure 1(b)-(c) reveal that the response has the shape of LNM-1 along the backbone and there are minimal contributions from higher harmonics observed in Figs. 1(f) and 1(g). In this regime, the dynamic response is clearly a nonlinear continuation of LNM-1. Along the internal resonance, a strong coupling is observed between LNM-1 and LNM-3 as seen in the deformation shapes of Points 3 and 4 in Fig. 1(d) and Fig. 1(e). The strength of the fifth harmonic increases as the response contains more energy along the internally resonant branch and the deformation of the beam transitions from being dominated by LNM-1 shape to being dominated by LNM-3.

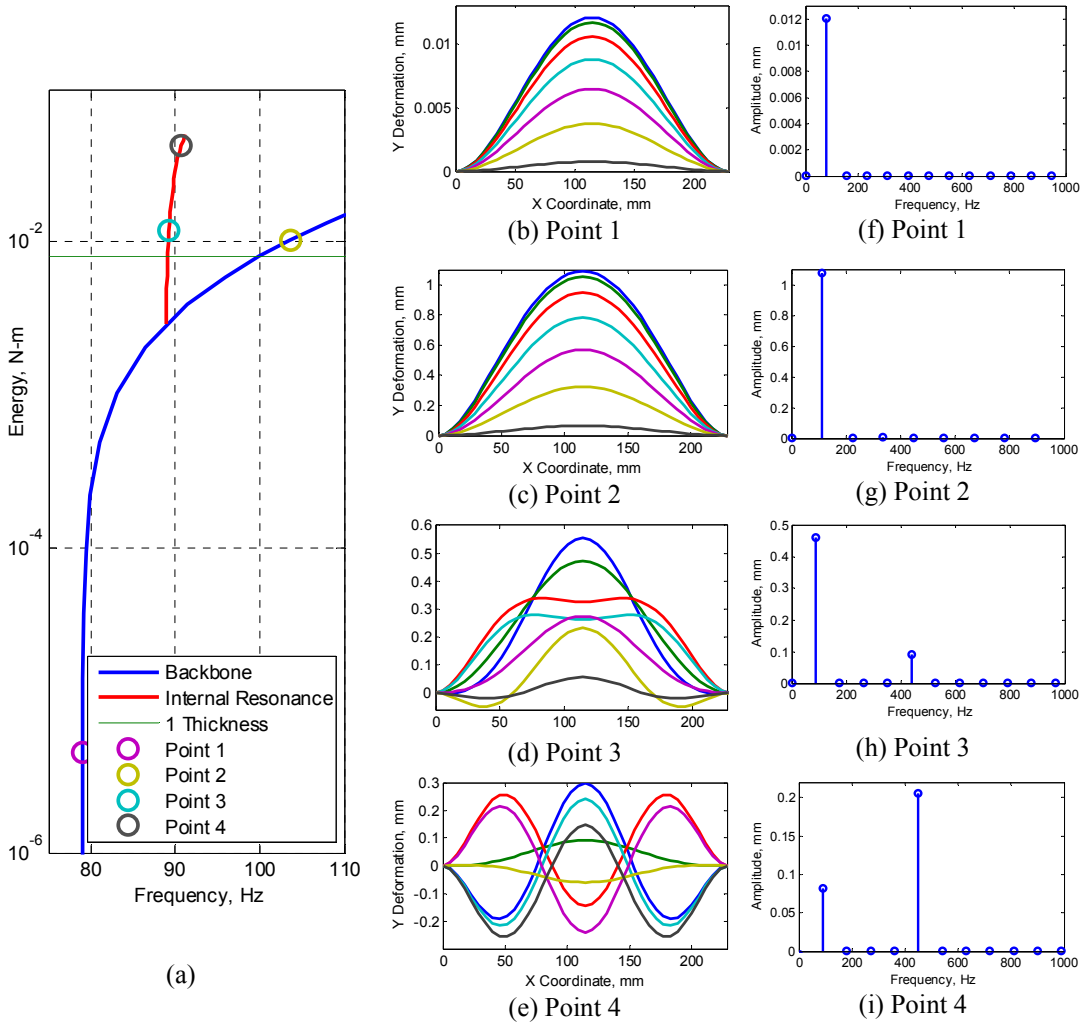

Figure 1: Numerical NNM 1 for flat clamped-clamped beam- a) Frequency-energy plot, b-d) Deformation shapes for a quarter period (— 0%, — 4%, — 8%, — 12%, — 16% , — 20%, — 25% of the period) at selected points along the FEP, e-g) FFT of the response at the center of the beam at those

same points

A NNM backbone emanates from each of the LNMs. Since LNM-3 is of interest in this study, NNM-3 as computed from the FEM is shown in Fig. 2 in a similar format. Once again, the horizontal line on the FEP in Fig. 2a marks the points where the structural deformation is equal to one beam thickness. It is important to note that over an order of magnitude more energy is required to achieve this deformation level when compared to NNM-1, since the deformation of NNM-3 is more complicated and the frequency/stiffness is higher. Throughout this range, LNM-3 dominates the deformation of the beam where the response is mono-harmonic with the fundamental frequency increasing by 52% over the range shown. Within this range, there are no internally resonant branches detected and NNM-3 is simply a nonlinear continuation of LNM-3. This conclusion is verified in Figs. 2(b)-(g), where low and high amplitude deformation shapes and FFT's are shown. A subtle broadening can be observed in the lobes of the mode shape, due to axial stretching from large amplitude deformations, but the shape retains the same basic character as amplitude increases. A similar broadening can be observed for NNM-1 in Fig. 1(c).

Figures 1 and 2 illustrate the wealth of insight that NNMs can provide into the response of a geometrically nonlinear structure such as this. The rest of this work is concerned with how one can measure NNMs such as these in order to characterize a structure or validate a computational model.

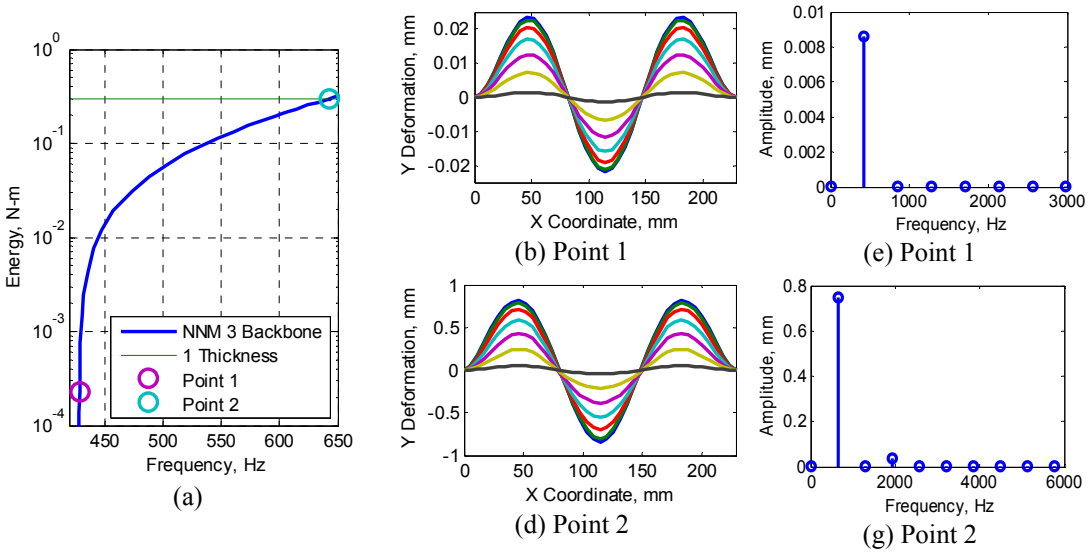

Figure 2: Numerical NNM 3 for flat clamped-clamped beam- a) Frequency-energy plot, b-d) Deformation shapes for a quarter period (— 0%, — 4%, — 8%, — 12%, —16% , — 20%, — 25% of the period) at selected points along the FEP e-g) FFTs of selected points along the FEP

2.1.3 Measuring NNMs with Force Appropriation

The industry standard phase lag criterion, which is reviewed in the appendix, only holds for LNMs, yet Peeters et al. presented an extension in [22] by which an undamped NNM can be isolated with force appropriation. This extension holds for a system with linear damping and nonlinear stiffness, which can be described by the following equation of motion:

$$\mathbf{M}\ddot{\mathbf{x}}(t) + \mathbf{f}_{\mathbf{d}} + \mathbf{f}_{\mathbf{nl}} = \mathbf{f}_{\mathbf{in}}(t) \tag{2}$$

Where the forced EOM defined previously have been augmented with the nonlinear restoring force vector, $\mathbf{f}_{\mathbf{nl}}$ which is only a function of displacement $\mathbf{x}(t)$. Using the method of harmonic balance [9], it can be shown that $\mathbf{f}_{\mathbf{nl}}$ will induce harmonics in the response at integer multiples of

the forcing frequency. Therefore it is beneficial to express the structural response as a sum of complex exponentials (a single term sufficed in Eqn. (16) for the linear system):

$$\ddot{\mathbf{x}}(t) = -\sum_{m=1}^{\infty} \mathrm{Re}\left((m\omega)^2 \mathbf{X_m} e^{i(m\omega t-\theta)}\right); \qquad \mathbf{x}(t) = \sum_{m=1}^{\infty} \mathrm{Re}\left(\mathbf{X_m} e^{i(m\omega t-\theta)}\right) \tag{3}$$

Similarly, under this assumption of harmonic motion, the damping force becomes:

$$\mathbf{f_d} = \sum_{m=1}^{\infty} \mathrm{Re}\left(i\left(m\omega\mathbf{C} + \mathbf{D}\right)\mathbf{X} e^{i(m\omega t-\theta)}\right) \tag{4}$$

Therefore, a NNM is appropriated when:

$$\mathbf{f_d} = \mathbf{f_{in}}(t) \tag{5}$$

Simply stated, the response of a structure approximates a NNM when the forcing function exactly cancels the damping forces in the structure. Furthermore, since the damping force is multi-harmonic, the input force must be as well. Then the phase condition must hold for all harmonics of the response. In practice one cannot apply a force that exactly cancels damping, so the goal is to apply a force that approximately isolates a NNM. In this work we apply the force at only a single point, denoted point n, and consider N_f harmonics, so the j^{th} element of the input force becomes the following:

$$f_{in}(t)_j = \begin{cases} \sum_{k=1}^{N_f} A_k \sin(k\omega t) & j = n \\ 0 & j \neq n \end{cases} \tag{6}$$

As was done in the Appendix, one can use the energy balance technique [38, 39] to find a force that puts the same amount of energy into the structures as is dissipated by damping. Because the sine functions are orthogonal over the fundamental period, T, when this is substituted into Eqn. (24), one obtains a sum of terms that give the contribution of each harmonic in the force to $E_{in/cyc}$.

$$\int_0^T \dot{\mathbf{x}}(t)^* \mathbf{C} \dot{\mathbf{x}}(t) dt = \sum_{k=1}^{N} A_k \int_0^T \dot{\mathbf{x}}_n(t)^* e^{ik\omega t} dt \tag{7}$$

In summary, given the known NNM motion, $\dot{\mathbf{x}}(\mathbf{t})$, and damping matrix, $\mathbf{C}$, the multi-point damping force, $\mathbf{C}\dot{\mathbf{x}}$, can be computed. From this, coefficients, A_k, of a multi-harmonic, single-point force can be determined that would input the same energy per cycle when the structure oscillates in the NNM of interest. This relationship explains why one can isolate a NNM by applying a single-point force, and it was also used in this work to numerically determine the forced responses needed to isolate a NNM in the simulation model. In practice the NNM is not known a priori, so one will generally have to tune the input until an NNM is isolated. Below we describe a simple strategy whereby one can observe how successive changes in the amplitude and fundamental frequency of the input force can be made to isolate the NNM of interest.

For either of the damping models described in the Appendix the damping force lags the displacement of the structure by 90 degrees, or it will be in phase with the structure's velocity.

The input force and response velocity can often both be measured at the point at which the structure is excited, and so one can use them to construct a simple indicator of the quality of the appropriated force by plotting the input force versus the velocity at the input location. One can use Green's theorem to show that the area enclosed on a force-velocity plot such as this goes to zero if all harmonics of the force and velocity are in phase. Hence the area enclosed by the curve provides an excellent indicator of the phase condition, and one which is easy to display in real time using an oscilloscope. The practical value of this indicator will be demonstrated in the simulation and experimental results that follow.

In order to find a the evolution of an NNM along a branch, this appropriation process can be repeated at subsequent frequency and amplitude levels until the branch of the desired NNM is identified. Since each point along the NNM corresponds to a time invariant periodic response of the structure, the measured force and response time series can be decomposed using a discrete Fourier transform, but one must take care to choose the sample increment and period carefully to avoid leakage; in practice, this will usually require re-sampling the signal. In this work the authors chose, instead, to use least squares to fit a multi-sine to the force and response at the dominant harmonics observed. Then the phase of all harmonics of the force and response are easily computed and can be used to check the phase condition. However, the examples presented here show that these phase measures can be overly sensitive and difficult to interpret. Instead, it is more convenient to use the *NNM Appropriation Indicator* (NNMAI) that was developed in [23]:

$$\Delta_{NNM} = \frac{1}{N_f} \sum_{k=1}^{N_f} \frac{\mathrm{Re}\{\mathbf{X}_k\}^{\mathrm{T}} \mathrm{Re}\{\mathbf{X}_k\}}{\mathbf{X}_k{}^{\mathrm{H}} \mathbf{X}_k} \tag{8}$$

Where N_f is the number of harmonics included in the indicator and $\Delta_{NNM} = 1$ for a perfectly appropriated mode. The tools available to aide in isolating an NNM are summarized in the table below.

Table 1: Summary of metrics which are used in this work to isolate an NNM. The values in the table correspond to the condition at resonance, or when an NNM has been isolated.

response type	phase lag relative to force	characteristic of a **force vs. response plot** when an NNM is isolated	NNMAI
displacement	90°	roughly elliptical (not used in this work)	1
velocity	180°	area enclosed approaches zero	1
acceleration	270°	roughly elliptical (not used in this work)	1

Throughout the rest of this paper, the phase of velocity relative to force will be the primary focus and the NNMAI, Δ_{NNM}, will be shown to be an excellent metric for assessing whether one is close to an NNM.

2.1.4 Numerical Example of Stepped Sine Measurement of NNM

The proposed approach will first be demonstrated numerically for the flat beam whose NNMs where shown previously. For this investigation, a Modified Crisfield integration technique is used to integrate the equations of motion to find the forced dynamic response of the flat beam when subjected to a single point harmonic excitation at the center of the beam. This integration can be prohibitively time consuming for a full order FEM, so the nonlinear reduced order model (NLROM) of the beam that was developed and verified in [20], was used to estimate the forced response. The theory underlying this type of NLROM is detailed in [36]. In summary, a model is sought in terms of the modal coordinates, q_r, which are related to the physical displacements as:

$$\mathbf{x}(t) = \sum_{r=1}^{N_r} \psi_r q_r(t) \tag{9}$$

where ψ_r is the r^{th} eigenvector of the conservative system linearized about an equilibrium of interest. Using this transformation and assuming viscous modal damping, Eqn. (2) can be recast as:

$$\ddot{q}_r + 2\zeta_r \omega_r q_r + f_{nl}^r\left(q_1, q_2, ..., q_{N_r}\right) = \psi_r^{\mathrm{T}} \mathbf{f_{in}} \tag{10}$$

where ζ_r and ω_r are the r^{th} modal damping ratios and eigenvalues of the structure. The modal damping ratios used in the simulation model considered here were identified using a single input modal hammer test and were assumed to be constant (i.e. not amplitude dependent) in the simulations. Additionally, the nonlinear modal restoring force, f_{nl}, is expressed as:

$$f_{nl}^r\left(q_1, q_2, ..., q_{N_r}\right) = \sum_{i=1}^{N_r} C_i^r q_i + \sum_{i=1}^{N_r}\sum_{j=1}^{N_r} B_{ij}^r q_i q_j + \sum_{i=1}^{N_r}\sum_{j=1}^{N_r}\sum_{k=1}^{N_r} A_{ijk}^r q_i q_j q_k \tag{11}$$

where the nonlinear stiffness coefficients are represented by C (linear), B (quadratic), and A (cubic) terms. These nonlinear stiffness coefficients were found by applying a series of static loads to the FEM, and using the resulting responses to solve a least squares problem, i.e. using the applied loads procedure [40] otherwise termed the Implicit Condensation method [36]. The model used in this work contains six modes, LNMs 1, 3, 5, 7, 9, and 11.

Once the reduced model had been created, the response was simulated and then the forcing frequency was stepped slowly near a NNM until an appropriated response was found. The force-velocity plot was used as an indicator of the phase condition as shown in Figs. 3 and 4 for two points identified on the numerical NNM which represent: a strongly nonlinear case (Point 2 in Fig. 1), and an internally resonant case (Point 3 in Fig. 1).

The results for Point 2 can be seen in Fig. 3. In addition to the force-velocity relationship, Fig. 3a, NNMAIs were calculated for the fundamental frequency of the input and all harmonics of the response and are given in the figure's caption. Each color corresponds to an increase in input frequency until the NNMAI is close to 1 while the input force amplitude was held constant. As seen in Fig. 3a and Fig. b, the response amplitude increases with increasing frequency as the forcing frequency becomes closer to the resonant frequency. To provide a comparison with Fig. 1c, the deformation over a quarter of a cycle of the appropriated response (NNMAI = 0.9999) is shown in Fig. 3c. The forced response can be seen to be a good approximation of the NNM-1 deformation shown in Fig. 1c. It is also interesting to note that the force-velocity trace is not a line but curves slightly at the ends as the NNM is reached due to the higher harmonics that are present in the response (which come about due to the stiffness nonlinearity). If the system were linear, the force-velocity relationship would be a line.

The response at Point 2 was dominated by a single-harmonic, so only one harmonic was needed in the input force to fully appropriate the response of the beam.

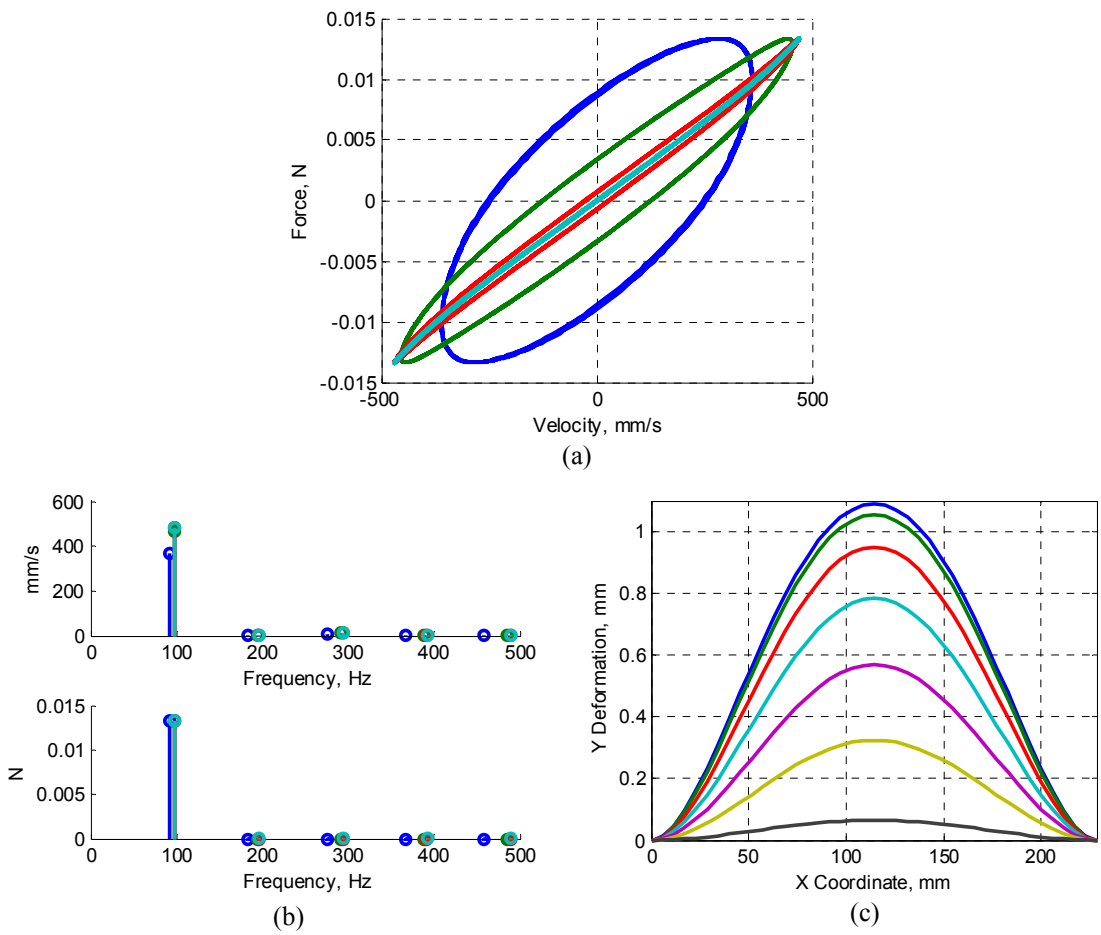

Figure 3: Appropriated force for Point 2. a) Input force versus response velocity, and b) Amplitude of force and velocity Fourier coefficients at points where the NNMAI values were (─0.5671, ─0.9358, ─0.9972, ─1.000), c) Deformation shapes for a quarter period (─0%, ─4%,─8%, ─2%, ─16% , ─20%, ─25% of the period)

Continuing to Point 3, which is on an internal resonance, a strong coupling is observed between LNM-1 and LNM-3 as previously discussed. Due to this coupling, higher harmonics were found to be necessary in order to appropriate the beam's response on the NNM. The single-point multi-harmonic forcing needed was determined using Eqn. (7). As in the previous figure, the responses at various points approaching the internal resonance are shown in Fig. 4. Once again the area enclosed by the force-velocity relationship in Fig. 4a does not simply follow a line in the force-velocity plane, yet while the curve is complicated the area enclosed by the curve decreases as the response approaches the true NNM confirming that the force-velocity plot is a good visual indicator of the quality of the appropriated response. The fifth harmonic of the response increases substantially as the driving frequency approaches the NNM frequency.

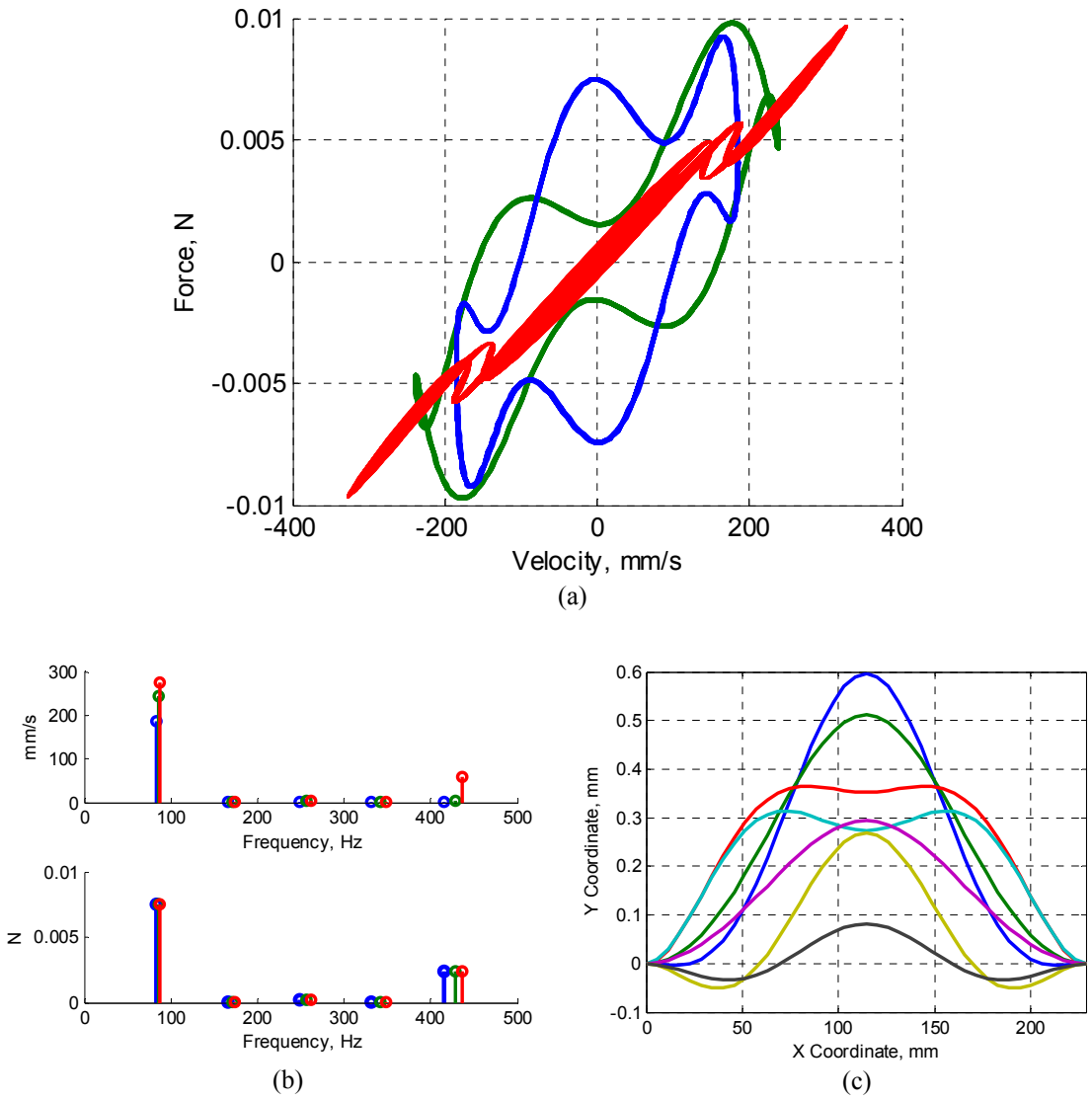

Figure 4: Appropriated force for Point 3. a) Input force versus response velocity, and b) Amplitude of force and velocity Fourier coefficients at points where the NNMAI values are (─0.5153, ─0.7747, ─1.0000), c) Deformation shapes for a half of a period at (─0%, ─4%, ─7%, ─11%, ─14% , ─18%, ─25%) of the period

In a simulation such as this it is trivial to compute the phase of the response compared with the phase of the input force and to compute the NNMAI. However, while the phase of the first harmonic was informative, it was challenging to make sense of the phase of the higher harmonics. To illustrate this, the phases computed at the points shown in Figs. 3 and 4 are presented in Tab. 2. Because the "measured" forcing will typically not be a pure sinusoid, the phase of all harmonics of the response were first corrected to account for the time delay that would make the fundamental harmonic of the input force a pure sinusoid. As previously discussed, one expects every harmonic to have a phase of 0° or 180° if the response is perfectly appropriated with the input force. For the cases shown in Figs. 3 and 4, it is interesting to note that although a single harmonic input force is used for Points 1 and 2, the higher harmonics of the response mostly approach this 0° or 180° relationship as the NNM is approached (and the NNMAI increases), but the phases in certain harmonics are as large as 90° even when the

NNMAI is quite high. This is explained by the fact that these harmonics have negligible amplitude in the response; the NNMAI automatically considers both amplitude and phase and hence seems to be a more robust metric than the phase lag.

Table 2: Frequency, NNMAI, and Phase Lag relative to force for Numerically Appropriated NNMs. The cells colored cyan are the frequencies at which the forcing harmonic was nonzero

Test Description		Fundamental Frequency	NNMAI	Harmonic Number						
				1	2	3	4	5	6	7
Point 2	1	91.6	0.567	41.1	151.7	123.2	214.1	31.8	53.7	126.0
	2	97.0	0.935	14.7	196.8	44.2	50.9	254.0	110.6	-76.1
	3	97.9	0.997	3.02	184.9	9.2	1.05	195.7	-27.6	201.7
	4	97.9	1.000	-0.24	179.5	-0.58	-1.64	179.4	-2.87	179.0
Point 3	1	83.0	0.515	44.1	126.5	131.4	-84.4	187.7	262.1	256.5
	2	85.6	0.774	28.3	136.4	85.2	139.4	3.41	199.6	58.5
	3	87.2	1.000	4.58	163.0	16.1	244.7	6.58	-6.7	15.9

In the experiments that follow, there was some doubt as to whether the phase of the input force could be precisely measured, and in a ring down experiment (as was used in [22] and as will be shown later), the forcing is zero so it is beneficial to consider whether the relative phases between the response harmonics can be used as an indicator. In this spirit, Tab. 3 shows a comparison between the phase of the fundamental harmonic of the response and all of the higher harmonics for all of these cases. If the NNM in question is synchronous, then the harmonics again should approach 0° or 180°. The results show that, for the cases considered, the phases do align as expected as the frequency approaches that of the true NNM.

Table 3: Relative Phase Lag between response harmonics for Numerically Appropriated NNMs. The cells colored cyan are the frequencies at which the forcing harmonic was nonzero.

Test Description		Harmonic Number						
		1	2	3	4	5	6	7
Point 2	1	0	110.59	82.09	173	-9.3	12.6	84.87
	2	0	182.13	29.49	36.18	239.33	95.94	-90.83
	3	0	181.94	6.18	-1.97	192.65	-30.68	198.73
	4	0	179.73	-0.34	-1.4	179.65	-2.63	179.25
Point 3	1	0	82.41	87.28	-128.54	143.63	218.03	212.42
	2	0	108.1	56.92	111.12	-24.92	171.32	30.23
	3	0	158.46	11.57	240.17	2	-11.28	11.41

2.1.5 Simulated Free decay Measurement of a NNM

As mentioned previously, the stepped sine approach is time consuming since the NNM must be isolated at each amplitude of interest. For systems exhibiting light damping, one might be able to find a high amplitude forcing that drives the system into one NNM and then measure the damped free decay of the system as described in [22]. It should be noted, however, that the authors found that this was difficult to do for the structures studied here. In order to excite an NNM the authors found it far easier to begin near resonance at low forcing amplitude and then to slowly increase both the force and the forcing frequency. In any event, in order for the free decay measurement to approximate an NNM several assumptions must be made about the dynamics of the structure. First, one must consider the damped nonlinear mode definition developed by Shaw

[41] and Jiang et al [14]. In that description, a NNM can be considered an *invariant* manifold, that describes the evolution of a pair of state variables in linear modal phase space. Note that to describe interactions of modes one must retain a pair of coordinates, (e.g. modal displacement and velocity), for each mode involved in the NNM response, complicating the interpretation. Due to the *invariance* property of these manifolds, a motion that initiates on the manifold will remain on it for all time. In practice the motion will never initiate precisely on the manifold, but if the damped NNM is an attractor of the damped free response then the motion will tend to decay along the manifold. Finally, the damping should be light so that the damped manifold is well approximated by the undamped manifold. Under these conditions the free decay of a system initiated on a damped NNM can be considered an approximation of the undamped NNM manifold. Since fundamental frequency in the free response changes with time, more complex signal processing techniques, such as the Wavelet Transform [42] and Hilbert Transform [43], are needed to interpret the results. An interesting contribution to this type of signal processing, applied to the identification of NNMs of structures, can be found in [44].

The Wavelet toolbox in MATLAB® was used here, with a Morlet wavelet, to examine the frequency and amplitude content of a decaying response of the flat beam, measured at the midpoint. A decay for the fully appropriated responses at Points 2 and 3 were simulated by removing the input force and calculating the free response as the amplitude decayed from this initial state. For Point 2, the time series and the Wavelet Transform are presented in Figs. 5a and 5b. Two harmonics are initially observed in this response at 110.7Hz and 335.7Hz corresponding to a 3:1 harmonic interaction; however, the fundamental harmonic dominates the response by more than an order of magnitude when compared with the third harmonic. For the decay initiated at Point 3, the wavelet transform, shown in Fig. 5d, shows two dominant frequencies in the response at 85.91Hz and 430Hz corresponding to the first and fifth harmonics of NNM-1. Based on this information alone, one cannot tell whether these responses have decayed along an NNM. It is therefore helpful to compare the true NNM-1 with the results of these free decay simulations and with the stepped-sine simulations.

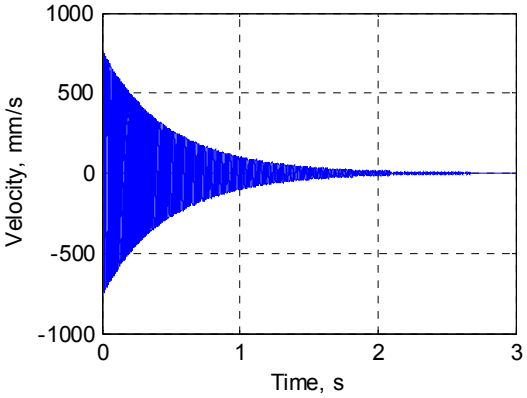

(a) Point 2

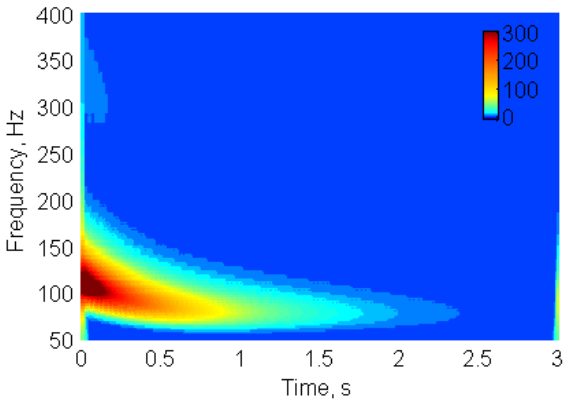

(b) Point 2

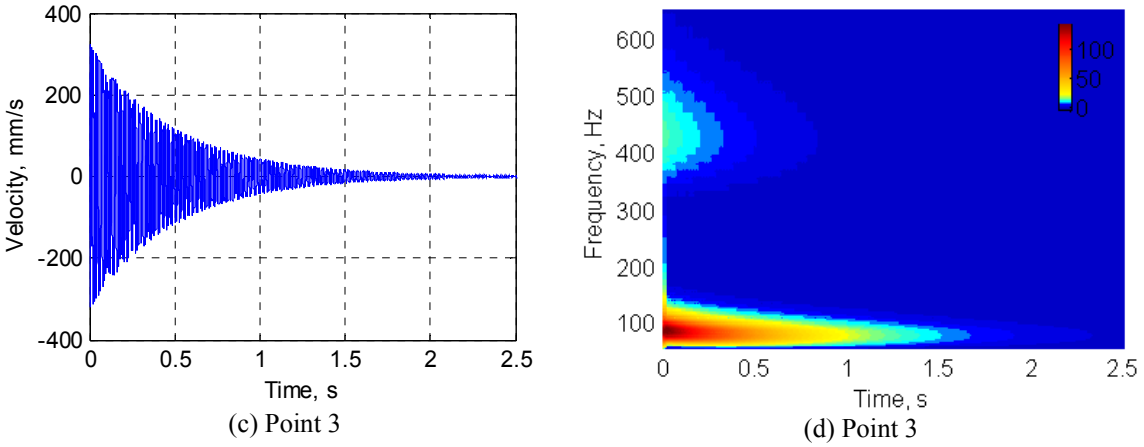

Figure 5: Wavelet analysis of free decay of appropriated NNMs. a) Time series and b) Wavelet decay of NNM appropriated at Point 2. c) Time series and d) Wavelet decay of NNM appropriated at Point 3

Figure 6 compares the stepped-sine and free decay estimates with the true NNM computed by AMF. Notice that the vertical scale is now in maximum deformation because it is not convenient to estimate energy from measurements. It should be noted that, with this change from energy to maximum displacement, the internal resonance branch now shows a decrease in the maximum deformation experienced by the structure, while it was shown before that there was an increase in response energy along the internal resonance branch. This is due to the internal resonance branch being dominated by LNM-3 which is a more complicated deformation resulting in greater response energy even though the maximum displacement decreases. It is also interesting to note that the maximum deformation of the center point crosses the backbone branch, while this does not occur in the frequency-energy plot.

The responses found using stepped-sine excitation were analyzed using Fourier series techniques and are shown with markers. The instantaneous amplitude and frequency of the decaying response was determined using the Hilbert Transform [43] and is shown with dashed lines. The decay that initiated from Point 2 is shown with a gold dashed line and can be seen to overlay well with the true backbone. The free decay seems to produce a good estimate of NNM-1 even though the response passes near the bifurcation point where the internal resonance occurs. The decay initiated at Point 3, shown with the dashed cyan line, also follows the backbone well even though it was initiated on the internal resonance (but near the backbone) and its response initially contained a significant 5^{th} harmonic component. The starting point of this decay is shown as a cyan circle. An additional decay experiment was also performed at a higher energy starting at Point 4 and is shown with the dashed black line. This decay does not follow the NNM backbone but tracks a course through the frequency-maximum amplitude space that is separate from the NNMs. Finally at much lower energies it converges to the NNM-1 backbone. This example illustrates a potentially important limitation to the free decay technique when an NNM exhibits strong modal coupling.

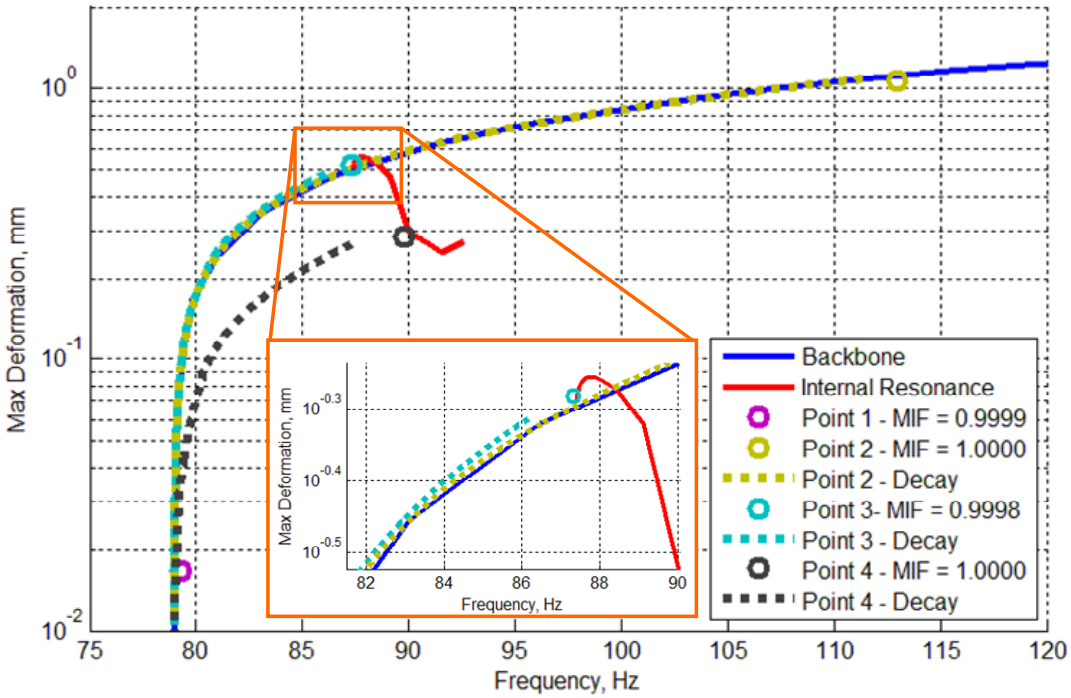

Figure 6: Comparison of NNM measurement techniques.

3 Experimental Application to a Clamped-Clamped Flat Beam

3.1 Structure Description

The structure used for the experiments presented here is a precision-machined feeler gauge made from high-carbon, spring-steel in a clamped-clamped configuration as shown in Fig. 7. The random response of this same hardware was previously studied in [45]. The beam has a nominal effective length of 228mm, a width of 12mm, and a thickness of 0.76mm. It is important to note that all presented dimensions are nominal and subject to variation from clamping and stress variations from machining process to obtain the desired thickness. Prior to clamping, the beam was prepared for three dimensional digital image correlation (3D-DIC) and continuous-scan laser Doppler vibrometry (CSLDV) as discussed in [46] and shown in Fig. 7. The clamping force was provided by four 6.35-28 UNF-2B bolts tightened to 9 N-m from left to right. After clamping the beam to the fixture, a single-input single-output modal hammer test was performed on the beam so linear natural frequencies and damping ratios could be identified as well as a static 3D-DIC measurement so any initial geometry variations could be identified. Additionally, operational modal analysis and CSLDV [47] were used to determine the mode shapes of the beam. The natural frequencies and damping ratios of the first ten modes, identified from the modal hammer test, are shown in Tab. 4, and the first seven elastic bending mode shapes measured by CSLDV are shown in Fig. 8. The CSLDV method measures the mode shape twice as the laser sweeps forward and then backward, so deviations between the two measurements give an indication of the measurement error.

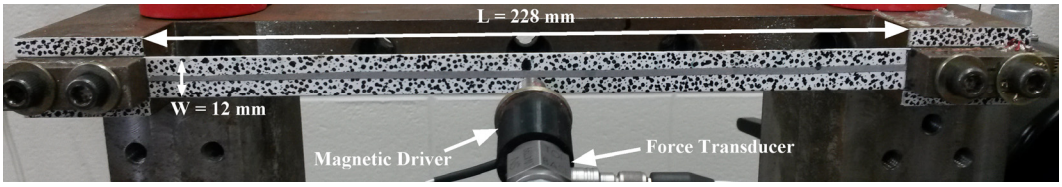

Figure 7: Photograph of Beam Specimen

Table 4: Linear (low amplitude) natural frequencies of flat clamped-clamped beam

	Mode 1	Mode 2	Mode 3	Mode 4	Mode 5	Mode 6	Mode 7	Mode 8	Mode 9	Mode 10
f, Hz	45.8	171.6	371.7	638.7	973.7	1376.5	1847.7	2387.2	2586.5	2994.7
$\zeta 1$, %	0.38	0.12	0.09	0.08	0.08	0.07	0.06	0.06	0.04	0.06

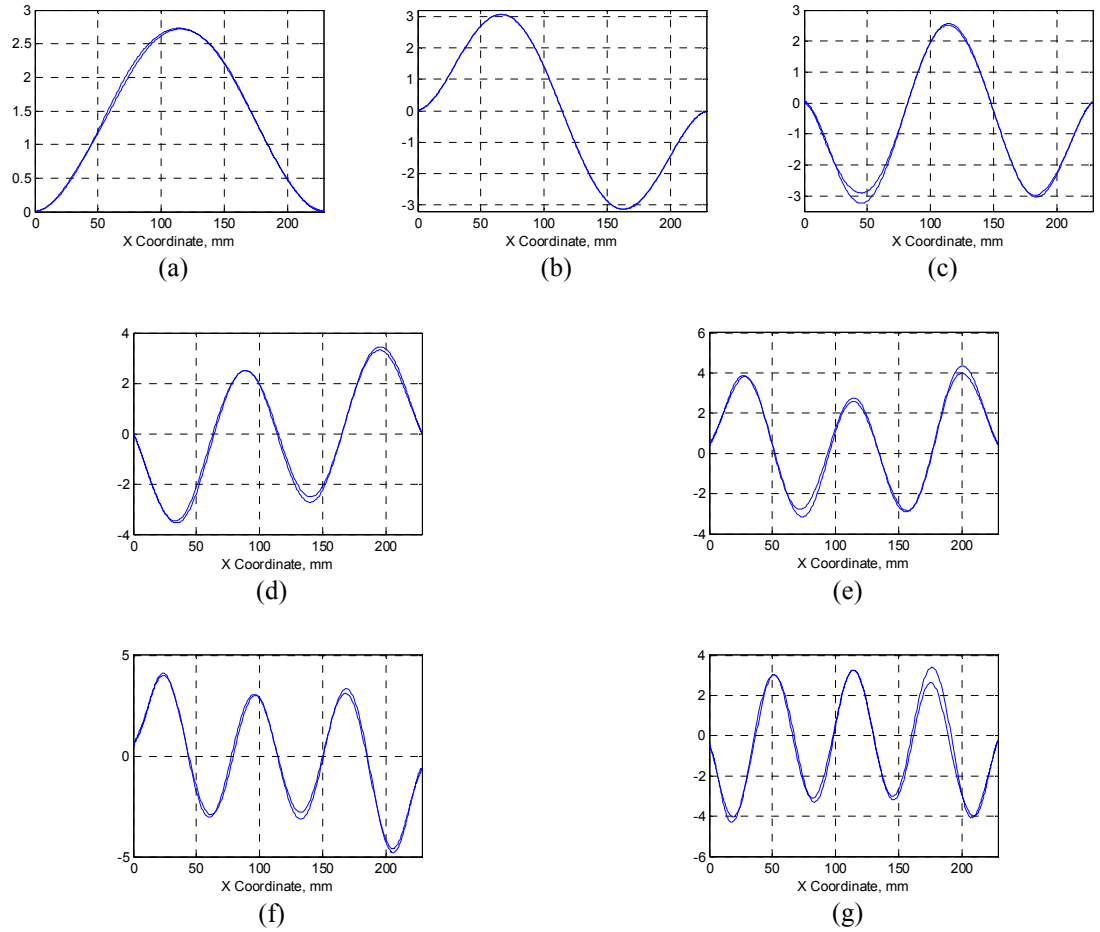

Figure 8: The first seven mode shapes of the beam. a-g) Modes 1-7

3.2 Experimental Setup

For this experimental setup, there are 3 systems: 1) exciter/controller, 2) Continuous-scan Laser Doppler Vibrometer measurement system, and 3) system for force appropriation:

1) Excitation of the structure was provided by a non-contacting magnetic driver powered by a Piezo Amplifier. The input force exerted by the magnetic driver cannot be directly measured, so instead a PCB force transducer was mounted between the magnetic driver and a solid base in an attempt to measure the reaction force of the driver. At lower forcing amplitudes,

complimentary results between the input voltage and measured force were found but a small phase difference was observed for some unexplained reason. At higher forcing amplitudes, the magnetic driver setup further contaminated the measured force as discussed later in Sec. 3.3, but a better alternative was not available.

2) Full-field dynamic measurements were taken using Continuous-scan laser Doppler vibrometry (CSLDV) and a 3D-DIC system was present but its results will not be presented here. Measurements from these two systems were compared in [48].

3) Prior to scanning, the single point laser Doppler vibrometer (LDV) was used to measure the response of the beam as it was subjected to a single frequency sinusoid at a specified excitation amplitude. The voltage input to the exciter was measured as well as the reaction force at the base of the magnetic driver. The velocity response and input voltage signals were measured in real time and displayed in a custom LabView program that also provided the capability of manually modifying the amplitude and frequency of each harmonic in the voltage sent to the amplifier.

3.3 Effect of Magnetic Driver on the Dynamics of the Beam

For light structures such as the beam investigated here, the apparatus used to apply an external force can modify the dynamics of the structure of interest. This has increased the interest in developing alternative methods of excitation, such as the magnetic driver which is used here. As previously mentioned, the magnetic driver used for the experimental setup can interact with the structure so care must be taken to understand how the magnetic driver will contaminate the results. The magnetic driver has a permanent magnet embedded in the inductor, so there is a magnetic field present even when no voltage is supplied. A low amplitude hammer test was performed on the beam before and after the magnetic driver was placed in front of the beam to characterize the linearized stiffness and damping effect that the magnetic driver has on the beam. The change in the identified natural frequencies and damping ratios before and after the magnetic driver was placed in front of the beam are presented in Tab. 5. The results show that the magnetic field has a greater effect on the estimated linear damping of the beam than the linear natural frequencies due to the presence of the magnetic field. For linear force appropriation, this will require a change in the force needed to achieve an appropriated response. It is also important to note that the natural frequencies and damping ratios changed by a comparable amount before and after the stepped-sine tests, presumably due to relaxation at the boundary conditions, temperature, or other effects, as discussed in [49].

Table 5: Percent Error of Identified Natural Frequencies and Damping Ratios when the magnetic driver is near the beam

Percent Error	Mode 1	Mode 2	Mode 3	Mode 4	Mode 5	Mode 6	Mode 7
f	2.07	0.88	0.36	0.26	0.02	0.17	0.12
ξ	-5.45	90.0	-35.0	0.0	-22.2	-6.7	0.0

Since the expected beam deflections are large, any nonlinearity from the driver could potentially contaminate the measured NNMs. In particular, since the magnetic driver is mounted on one side of the beam, the fluctuating magnetic field will asymmetrically load the structure causing the presence of unexpected dynamics. Therefore, To determine whether the voltage signal is representative of the input force, the exciter was used to excite a load cell mounted to a rigid base. The reaction force measured on the magnetic driver setup and the excited load cell were shown to compare well with each other and the input voltage as discussed in [49] so

measurements proceeded. However, during the measurements the reaction force was found to vary considerably from the input voltage. For example, Figs. 9a and 9b compare the measured force, voltage, and velocity of the structure at a low and high amplitude resonance responses similar to those that will be presented later. The input voltage closely resembles the response of the beam, but the measured reaction force exhibits a small phase shift for the low amplitude response and completely different characteristics for the large amplitude response.

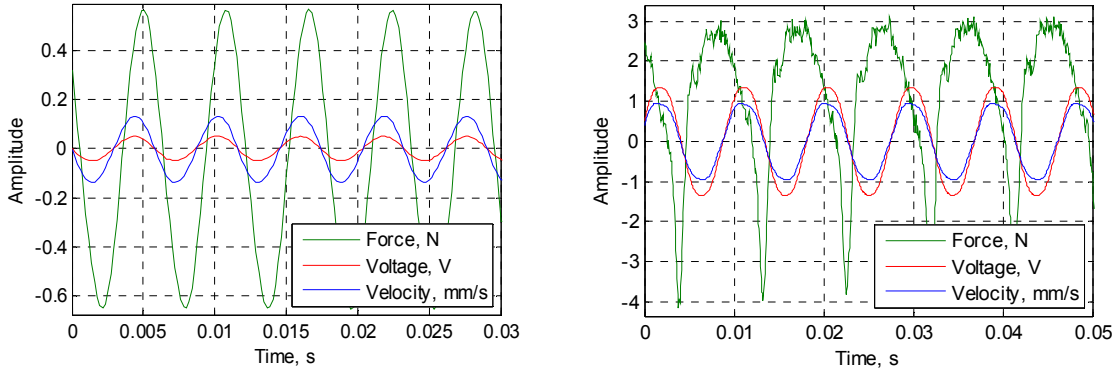

Figure 9: Comparison of force, voltage and velocity signals.
a) Low amplitude response. b) High amplitude response.

It appears that the magnetic driver induces a force on the beam that is not well characterized by the input voltage (which will be used later as a surrogate for the force in the appropriation experiments). However, the higher harmonics in the force do not seem to induce much deformation in the beam, and hence they may not contribute significantly to the energy input to the beam. To verify this, the energy that would be input by the measured reaction force was calculated using Eq. (22) with the integral evaluated numerically. Several harmonics are present in the measured force, so the energy was further decomposed into the contribution of each harmonic to the energy input. The process was then repeated at three points where appropriation results are presented, as elaborated in the next section, and the result is shown in Tab. 6. For the first three points, the first harmonic dominates the power input to the beam. At Point 3, which corresponds to an internally resonant NNM-1 branch, the power input by the fifth harmonic appears to have a significant contribution as well. In contrast, the second harmonic, which is responsible for much of the distortion in the measured force in Fig. 9b, contributes negligible power and hence its effect on the NNM can hopefully be ignored. Because the measured force is not trustworthy, in all of the results presented in the following section the input voltage will be used as a surrogate for the input force.

Table 6: Power Input to the Beam

	Harmonic 1	Harmonic 2	Harmonic 3	Harmonic 4	Harmonic 5	Harmonic 6	Harmonic 7
Point 1	$2.63\text{x}10^{-3}$	$7.34\text{x}10^{-5}$	$2.01\text{x}10^{-5}$	$9.76\text{x}10^{-7}$	$2.86\text{x}10^{-7}$	$9.09\text{x}10^{-8}$	$1.13\text{x}10^{-7}$
Point 2	$4.43\text{x}10^{1}$	$2.03\text{x}10^{-1}$	$6.29\text{x}10^{-1}$	$1.99\text{x}10^{-1}$	$-1.80\text{x}10^{-1}$	$-2.90\text{x}10^{-3}$	$-2.99\text{x}10^{-3}$
Point 3	$1.22\text{x}10^{1}$	$6.10\text{x}10^{-2}$	$-1.37\text{x}10^{-1}$	$1.69\text{x}10^{-2}$	$-1.33\text{x}10^{0}$	$3.30\text{x}10^{-2}$	$2.06\text{x}10^{-1}$

3.4 Experimental Example of Stepped Sine Measurement of NNM

As was done in the following section the results of force appropriation will first be highlighted at three points which, following the same nomenclature used in the previous section,

are thought to correspond, respectively to: a point at low energy, a point high up on the main NNM-1 backbone, and a point on the internal resonance. In each case a single-harmonic force was stepped up in frequency until the fundamental harmonic was nearly appropriated and additional harmonics were added to reduce the area enclosed by the voltage-velocity relationship and tune the shape of that curve.

At Point 1, three successive measurements were taken where a harmonic was added to the forcing function at each measurement. The added harmonic was selected to counter the strongest harmonic observed in the response. The results are shown in Fig. 10, where blue corresponds to a single harmonic force, green is a two harmonic force, and red is a three harmonic force. It is interesting to note that although higher harmonic content was added to the input force changing the shape of the voltage-velocity relationship considerably (Fig. 10a), the amplitudes of the second and third harmonics of the response, shown in Fig. 10b, remain very small. The second harmonic seems to reduce the area enclosed by the curve, but the third simply serves to linearize the force-velocity relationship. If the voltage is an accurate surrogate for force, then one would expect the case with two harmonics (in green) to produce a response closest to the underlying nonlinear mode, suggesting that the system is still somewhat nonlinear at this low amplitude. The addition of the third harmonic may or may not improve the result. This question is deferred until later when the resulting NNMAI metrics are presented (e.g. see Table 7).

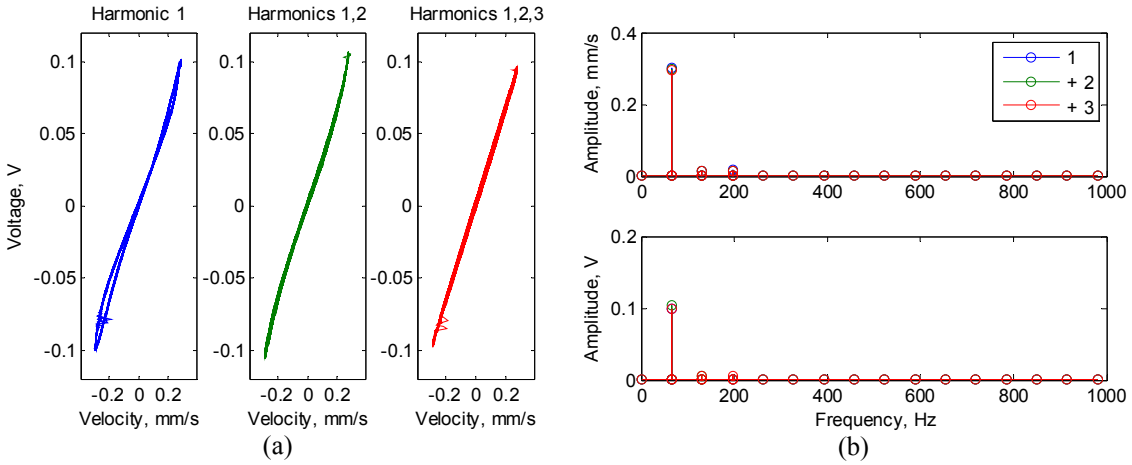

Figure 10: Appropriated force for Point 1. a) Voltage vs. Velocity, b) Amplitude of Fourier coefficients

This process was repeated for Points 2 and 3. The results for Point 2, which correspond to a strongly nonlinear point on the backbone of NNM-1, are shown in Fig. 11. Again, higher harmonics were added to the input force based on the harmonic content observed in the response. With the addition of two harmonics, the area enclosed by the voltage-velocity relationship approaches zero, as shown in Fig. 11a. For this strongly nonlinear response, a the third harmonic begins to stand out in the spectrum shown in Fig. 11b. As in the Point 1 case, the addition of further harmonics seems to cause the voltage-velocity relationship to approach a straight line.

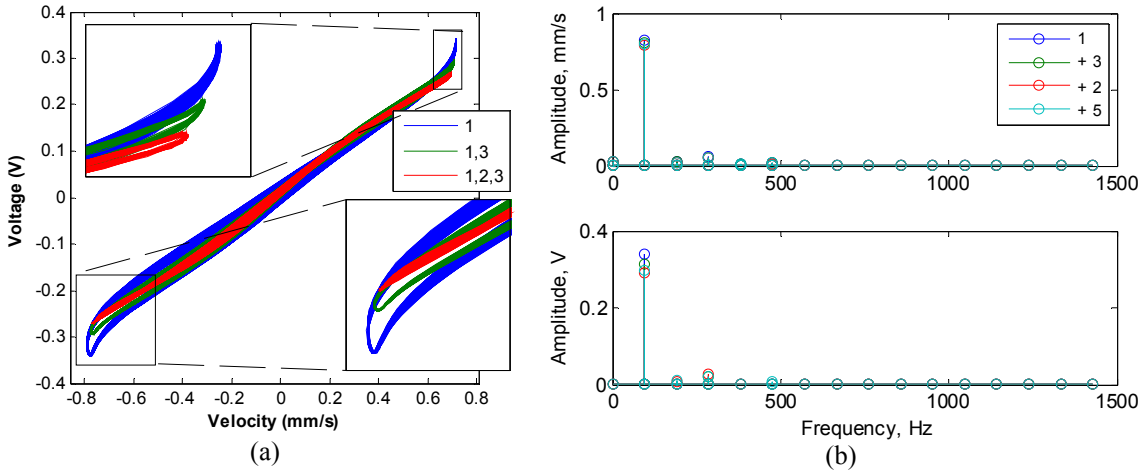

Figure 11: Appropriated force for Point 2. a) Voltage vs. Velocity, b) Amplitude of Fourier coefficients

The results for Point 3, on the internal resonance, are shown in Fig. 12. Here the voltage-velocity curve is far more complicated. The 5th harmonic seems to significantly reduce the area enclosed by the curve. Adding further harmonics seems to reduce the area further, but it also causes the relationship to be nearly linear. In the final appropriated response, the fifth harmonic is almost half the amplitude of the fundamental harmonic, showing a strong harmonic coupling of LNM-1 and LNM-3 as was seen in the finite element model. Qualitatively, the response characteristics match those of the simulated beam but the phase and NNMAI will need to be examined in detail to see which result provides the most accurate estimate of the NNM.

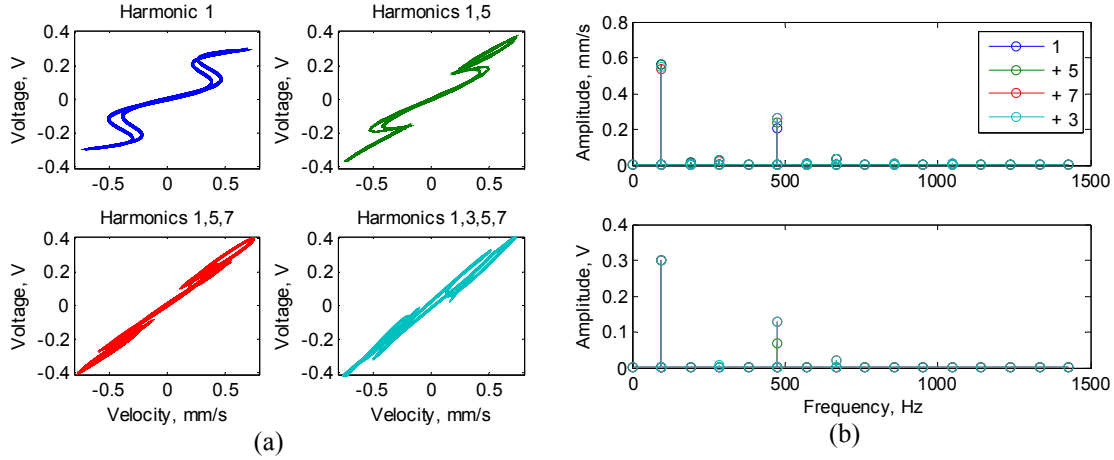

Figure 12: Appropriated force for Point 3. a) Voltage vs. Velocity, b) Amplitude of Fourier coefficients

As was done for the simulated experiments, the measured voltage and velocity were decomposed using a least squares multi-sine fit. The resulting complex Fourier coefficients were used to calculate the phase of the first several harmonics. For ease of comparison, the response harmonics were shifted to account for the phase of the fundamental harmonic of the input voltage. The phase of the voltage is thought to give an adequate, yet imperfect estimate of the phase of the induced magnetic field in the inductor which is related to the force input to the beam, as discussed

in Sec. 3.3. The phases of the harmonics of the response relative to the fundamental harmonic of the input voltage were computed and are shown in Tab. 7. The cells shaded with blue correspond to harmonics that were nonzero in the input voltage. It is immediately apparent that many of the harmonics show phases that are very far from the desired 0 or 180°. Particularly, the even harmonics tend to be near 90° whether or not a corresponding force had been applied. In particular, it seems that the 2nd harmonic need not have been added to the input force.

For Points 1 and 2 the phases are near 0 or 180° when the force includes only a single harmonic, and some improvement is seen as higher harmonics are added; however, some of the cases show that as additional harmonics are added, the phase gets worse. Even then, all of the cases shown for Points 1 and 2 seem to be well appropriated. For Point 3, as higher harmonics are added the phase of the 5th and 7th harmonics improve somewhat. The results presented here show that care must be taken when adding harmonics to the force. If the harmonics aren't needed they seem to artificially linearize the force-displacement relationship, making the estimate of the NNM less accurate.

Table 7: Phase relationships between the first harmonic of the Input Voltage and all harmonics of the measured response

Phase (°) Between Voltage and Response								
Test Description		Harmonic Number						
		1	2	3	4	5	6	7
Point 1	1	1.18	-91.87	177.74	88.51	-0.62	102.83	27.42
	2	1.05	-92.37	177.19	83.59	-4.41	88.85	58.86
	3	1.30	-91.86	177.97	86.11	-2.59	92.81	67.82
Point 2	1	2.14	-90.07	-177.65	94.06	-176.90	-75.11	4.87
	2	0.79	-93.01	178.34	89.44	176.50	-79.48	-4.22
	3	0.63	-93.25	177.73	89.62	175.64	-78.04	-4.46
	4	0.59	-93.49	177.67	89.18	175.40	-78.54	-5.23
Point 3	1	1.87	-89.96	-173.23	-113.58	-18.44	-107.99	163.15
	2	1.90	-90.07	-172.63	-110.74	-17.08	-107.89	164.51
	3	3.51	-86.57	-164.18	-108.60	-13.46	-103.35	171.77
	4	2.92	-87.95	-166.86	-108.87	-14.40	-104.66	169.54

As discussed previously, there is some doubt as to whether the phase of the voltage matched the phase of the force. To circumvent this, the relative phases between the response harmonics were considered as was done previously in Tab. 3 and the result is shown in Tab. 8. The *NNM Appropriation Indicator* (NNMAI) introduced in Eqn. (8) is also shown in Tab. **8**. Three NNMAIs were computed, each including a different set of harmonics: all harmonics 1 through 7, the odd harmonics, and the even harmonics. The maximum value of each NNMAI in each test is shaded in orange. The odd harmonics dominate the nonlinear response, as was shown in Figs. 10b, 11b, and 12b.

For any of the selected force distributions, the odd harmonics can be considered well appropriated (e.g. all NNMAI values are above 0.83) and confirm that the stepped-sine backbone is a good estimate of the NNM. In all three cases the results show that some of the higher harmonics that were added did not improve the estimate of the NNM. Fortunately, in the simulation section the frequency-amplitude behavior was shown to not be very sensitive to even relatively large changes in the NNMAI, so the measured NNMs should still be reasonably accurate.

Table 8: Phase relationships between the fundamental and higher harmonics of the response

Relative Phase (°) of Response to first harmonic											
Test Description		Harmonic Number							NNMAI		
		1	2	3	4	5	6	7	All	Odd	Even
Point 1	1	0.00	-94.23	174.21	83.79	-6.52	95.75	19.16	0.5398	0.9643	0.0091
	2	0.00	-94.47	174.04	79.40	-9.65	82.56	51.53	0.5406	0.8337	0.1743
	3	0.00	-94.45	174.09	80.93	-9.06	85.04	58.75	0.4738	0.8398	0.0162
Point 2	1	0.00	-94.35	175.93	85.50	172.40	-87.95	-10.11	0.5208	0.9867	0.0549
	2	0.00	-94.60	175.95	86.26	172.52	-84.25	-9.78	0.5586	0.9873	0.1300
	3	0.00	-94.52	175.83	87.08	172.47	-81.85	-8.91	0.5054	0.9884	0.0224
	4	0.00	-94.68	175.89	86.81	172.43	-82.10	-9.38	0.5841	0.9877	0.1805
Point 3	1	0.00	-93.69	-178.83	-121.05	-27.78	-119.19	150.07	0.5539	0.8834	0.2244
	2	0.00	-93.86	-178.33	-118.34	-26.57	-119.28	151.22	0.5533	0.8918	0.2148
	3	0.00	-93.59	-174.71	-122.65	-31.02	-124.43	147.18	0.5254	0.8581	0.1927
	4	0.00	-93.78	-175.61	-120.54	-28.98	-122.16	149.13	0.5212	0.8740	0.1684

3.5 Measured Backbone Curves

Before examining the measured NNMs, it is interesting to examine the free response as the beam decayed from Points 2 and 3 and their corresponding Morlet wavelet transforms, shown in Fig. 13. The decay was initiated at 106.98 Hz, after a 61.18 Hz shift in the first mode of the beam from its linear natural frequency, so it encompasses a response over a strongly nonlinear regime. The amplitude of the time signal decays smoothly but there is a sudden jump near 2.5 seconds. Similarly, the wavelet coefficients near the 5th harmonic of the response show a sudden increase at that same instant. At this instant in the decay, the response is near the internal resonance branch showing contamination between the NNMs. The higher harmonic content was still quite small and so it was disregarded when estimating the NNM backbone.

Figures 13c and 13d show the results for the decay that initiated at Point 3. For the decay from this point, the wavelet coefficients at the 5th harmonic are on a similar scale as the fundamental harmonic as seen in Fig. 13d.

Similarly, a decay experiment was performed on NNM-3. The wavelet transform shown in Fig. 13f shows only a single frequency response, with no higher harmonics clearly visible. However, there does appear to be an interaction with LNM-1, which can be seen near the bottom of the plot in light blue. This sub-harmonic content only occurs after the force has been turned off and its frequency does not change during the decay, so it could simply be due to a spurious excitation of linear mode 1 when the force is turned off. Since NNM-3 has a higher frequency, its response decays in a third of the time required for NNM-1 to decay. This makes it more challenging to accurately extract the backbone using the wavelet or Hilbert transforms.

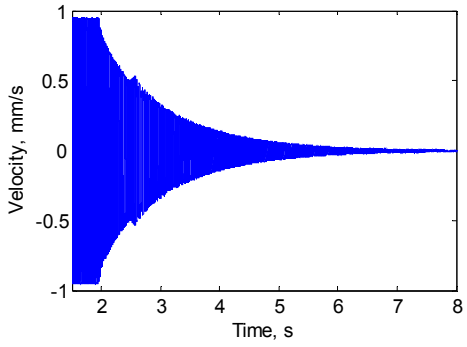

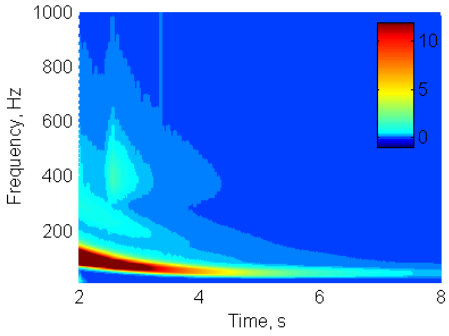

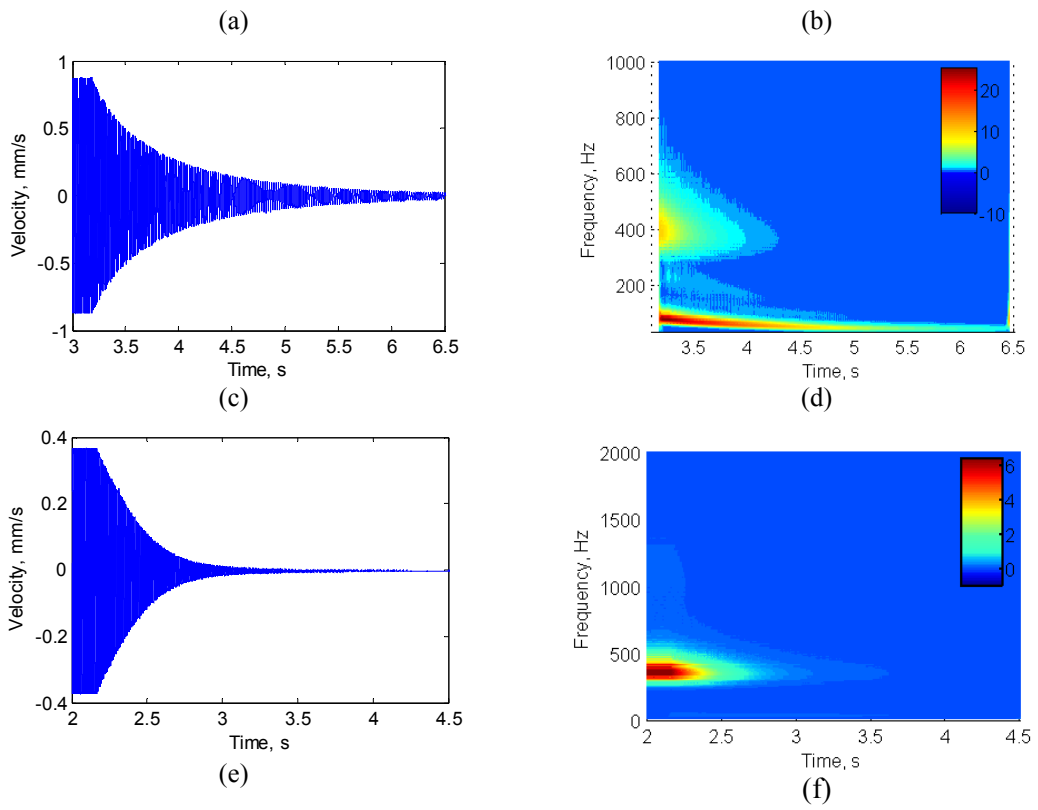

Figure 13: Time series and wavelet transform of the three experimentally measured free decays. a) Time series and b) Wavelet transform corresponding to the NNM-1 Point 2 decay, c) Time series and d) Wavelet transform corresponding to the NNM-1 Point 3 decay, e) Time series and f) Wavelet transform corresponding to the NNM-3 Point 2 decay.

These results were next used to estimate the backbone of NNM-1 and the result is shown in Fig. 14. The circles mark the results from the stepped-sine testing and the lines show the backbones extracted from the free decays using the Hilbert transform. The free decay initiated at Point 2 (blue) agrees very well at high amplitude, although it begins to deviate at low amplitude as the LNM is approached. The maximum difference between the two is 2.71 Hz, and this is similar to the difference between the backbone estimated from the stepped sine test and the linear natural frequency estimated in a hammer test. The maximum deviation in frequency between the stepped-sine and the decay from Point 2 is 4.25 Hz, occurring at the second lowest amplitude response point measured by the stepped-sine technique. This point is at a lower frequency then the point with the lowest amplitude and this could be a result of a spring-softening. This structure is known to be prone to softening behavior [49] and the magnetic exciter might also induce softening.

The stepped sine results show a plausible estimate of the internal resonance, although the points do not evolve as smoothly as one would expect. However, when a free decay was initiated from the point shown on this branch the measured amplitude was found to follow a seemingly arbitrary path in frequency and amplitude until it finally settles on the NNM-1 backbone. Note that the Hilbert transform algorithm induces an initial transient in the calculated frequency-amplitude relationship that was removed for a better fit. The start point of the free decay was added to the decay results based on the identified frequency and amplitude from the steady-state measurements, resulting in a discontinuity observed at the highest frequency of the internally resonant decay.

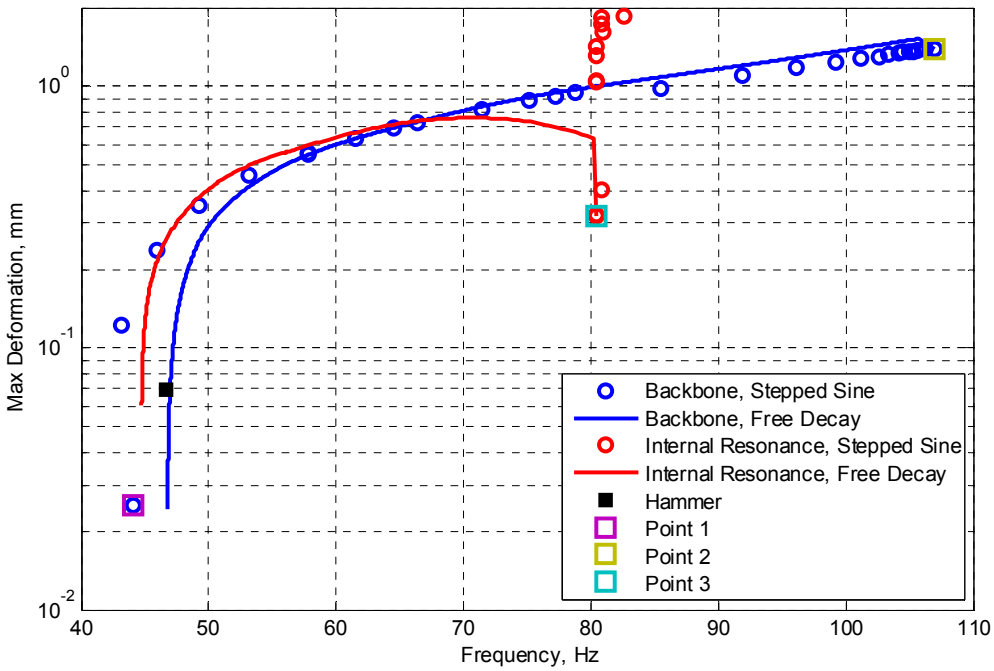

Figure 14: Frequency-Amplitude behavior of the NNM-1 backbone and internally resonant branch

Similar results are found for NNM-3, where only a single decay is needed to measure the backbone shown in Fig. 15. Due to limitations in the experimental setup, NNM-3 can only be measured to a smaller maximum deformation than was achieved for NNM-1. It should be noted that although the results between stepped-sine and free decay appear more scattered the maximum frequency error between the identified backbones is only 1.4% which is within the experimental error.

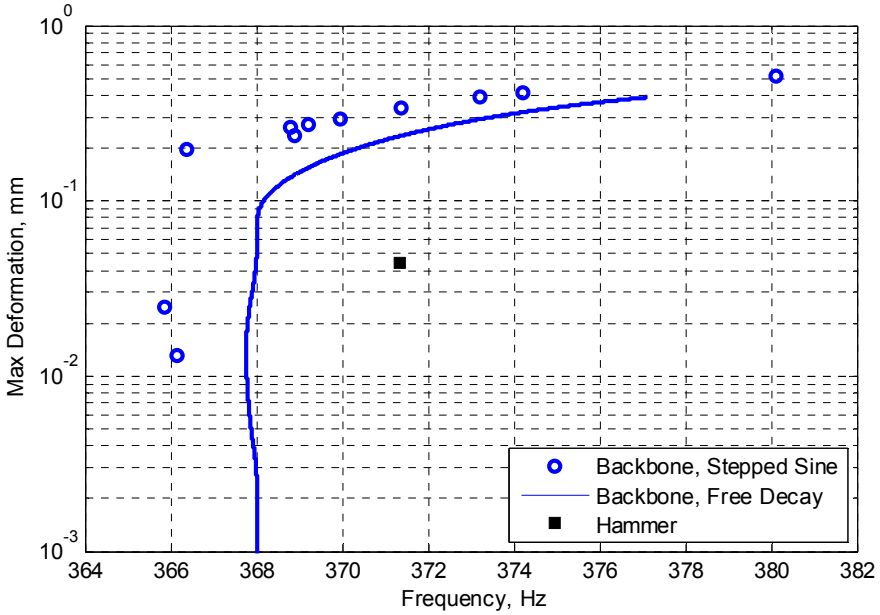

Figure 15: Frequency-Amplitude behavior of the NNM-3 backbone.

3.6 Full-Field Deformation Shapes along the measured NNM backbone

An additional benefit to the use of stepped-sine testing is the ability to easily implement advanced full-field measurement techniques to measure the deformation of a structure. This allows the full-field deformation shapes to be examined and compared with numerically calculated deformations. The CSLDV system mentioned previously was used to measure the deformation of the surface of beam along the line of retro-reflective tape shown in Fig. 7.

Again following the first three Points of the NNM shown in Fig.14, the deformation shapes of the experimentally measured NNM in the neighborhood of these three points is shown in Fig. 16. The deformation near Point 1, shown in Figs. 16(a) and 16(d), matches the expected deformation for a linear beam and harmonic content in the response is similar to that in the analytical NNM, as was shown in Figs. 1(b) and 1(f).

Point 2 shows a similar deformation pattern, but as the deformation approaches zero, a small skew is observed. Although this deformation is dominated by single harmonic and by LNM-1, the second and third harmonic also contribute as shown in Fig. 16(e).

The measured NNM near Point 3, shown in Fig. 16(c), shows the same interplay between LNM-1 and LNM-3 that was seen in the simulated results in Fig. 1(d),. The experimental measurement also shows a slight asymmetry in the deformation. The fifth harmonic also begins to contribute more to the response as expected.

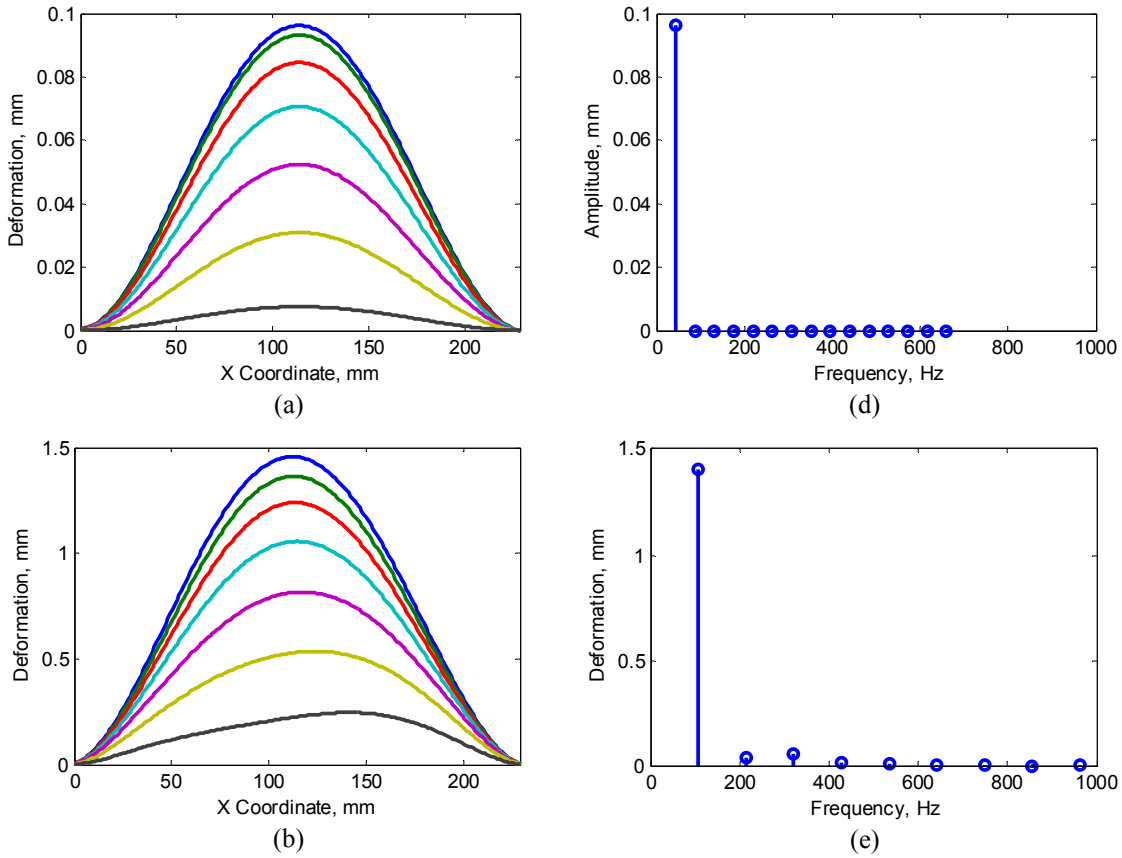

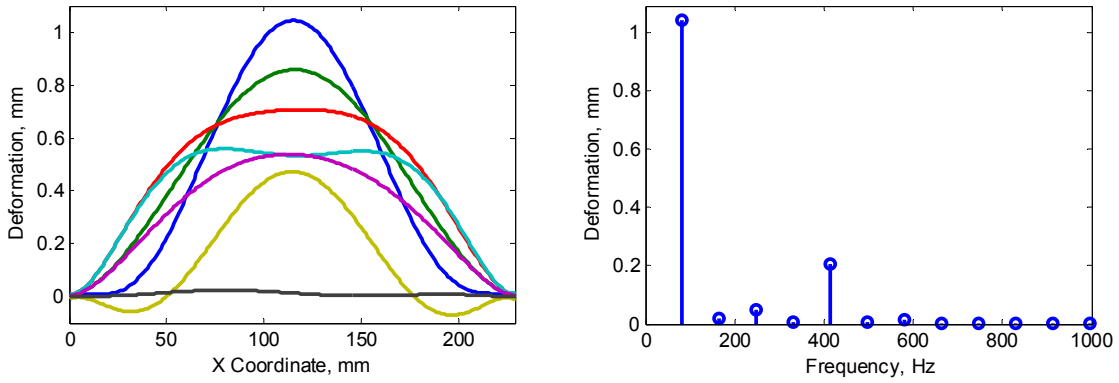

(c) (f)

Figure 16: Full-field deformations of experimentally measured NNM. a-c) Deformation shapes for a half of a period at (—0%, —4%, —7%, —11%, —14% , —18%, —25%) of the period. d-f) Fourier coefficients of the response at the center of a beam over a period of the response.

4 Conclusion

This work has shown that multi-harmonic forces can be used to experimentally isolate NNMs even on an internal resonance. In doing so, it is helpful to monitor a plot of the force versus velocity and then it becomes fairly intuitive to adjust the amplitudes of the harmonics in the force until the curve shows minimal area. However, the results presented here show that one can find several responses that seem to have minimal area yet do not satisfy the phase criterion equally, and so it is wise to also compute the nonlinear mode indicator or the phases of the response harmonics to check whether an NNM has been accurately isolated. Fortunately, the simulation results also showed that one can accurately estimate the frequency and amplitude/energy of an NNM even if there is considerable error in the mode indicator. Values of Δ_{NNM} as low as 0.5 can still be used to estimate the NNM frequency within only a few percent. It was also shown that the phases of the response harmonics can provide a good indicator of how close one is to an NNM, but they are more challenging to deal with because they are also very sensitive to small changes to the forcing and the weak harmonics tended to have spurious phases.

Another goal of this work was to compare stepped sine appropriation to the more convenient free decay method. The results showed that the free decay method provided comparable results when the response was initiated on the main backbone of an NNM. However, when initiated on an internal resonance the transient decay did not follow the backbone of the NNM, but instead decayed along a totally different path. There does not seem to be any easy way to query the free response to see whether it is still on a true NNM or not. In this regard the stepped sine method is preferred because one obtains a quantitative metric that can be used to evaluate the quality of each point. One additional benefit of the use of stepped-sine measurements is that it became easy to implement continuous-scan laser Doppler vibrometry (CSLDV) to measure the full-field deformation along the surface of the beam. The deformation shapes measured from the beam showed excellent qualitative agreement with the numerically calculated NNMs.

Admittedly, the structure studied here was fairly simple, but even then simulations have shown that the NNM backbones and the couplings between the underlying linear modes can be highly sensitive to the boundary conditions and to the initial shape of the beam. Hence, experimental measurements of the NNMs such as these are expected to be very valuable when updating the finite element model to better correlate with the actual test hardware. For more complicated structures, such as the skin panel of an aircraft, these tools are expected to be even more critical. In the future, it may even be possible to project the measured deformation onto the

experimentally identified linear modes, allowing one to develop a reduced order nonlinear modal model experimentally. This will be pursued in future work.

5 References

[1] D. J. Ewins, *Modal Analysis Theory, Practice, and Application*, Second Edition ed.: Research Studies Press Ltd., 2000.

[2] R. J. Allemang, and Brown, D.L., *Chapter 21: Experimental Modal Analysis*, 6th ed.: McGraw-Hill Book Company, 2008.

[3] G. Kerschen, and Golinval, J.C. (2015). *Experimental Modal Analysis*. Available: www.ltas-vis.ulg.ac.be/cmsms/uploads/File/Mvibr_notes.pdf

[4] G. F. Lang, "Matrix Madness and Complex Confusion... A Review of Complex Modes from Multiple Viewpoints," *Journal of Sound and Vibration,* vol. 46, 2012.

[5] W. T. Thomson, and Dahleh, M.D., *Theory of Vibration with Applications*, 5th ed. Upper Saddle River, New Jersey: Prentice-Hall Inc., 1998.

[6] J. H. Ginsberg, *Mechanical and Structural Vibrations Theory and Applications*: John Wiley and Sons Inc., 2001.

[7] R. C. Hibbeler, *Dynamics*, 13 ed. Upper Saddle River, NJ: Prentice Hall, 2010.

[8] F. Costanzo, Plesha, M.E., and Gray, G.L., *Statics and Dynamics*. New York, NY: The McGraw-Hill Companies Inc., 2010.

[9] K. Worden, and Tomlinson, G.R., *Nonlinearity in Structural Dynamics: Detection, Identification, and Modeling*. Bristol and Philadelphia: Institute of Physics Publishing, 2001.

[10] R. M. Rosenberg, "Normal Modes of Nonlinear Dual-Mode Systems," *Journal of Applied Mechanics,* vol. 27, pp. 263-268, 1960.

[11] G. Kerschen, M. Peeters, J. C. Golinval, and A. F. Vakakis, "Nonlinear normal modes, Part I: A useful framework for the structural dynamicist," *Mechanical Systems and Signal Processing,* vol. 23, pp. 170-194, 2009.

[12] A. F. Vakakis, "NonLinear Normal Modes and Their Applications in Vibration Theory: An Overview," *Mechanical Systems and Signal Processing,* vol. 11, pp. 3-22, 1997.

[13] W. Lacarbonara, Rega, G., Nayfeh, A.H., "Resonant Nonlinear Normal Modes Part I: Analytical Treatment for Structural One-dimensional Systems," *International Journal for Nonlinear Mechanics,* vol. 38, pp. 851-872, 2003.

[14] D. Jiang, Pierre, C., and Shaw, S.W.,, "The Construction of Non-Linear Normal Modes for Systems with Internal Resonance," *International Journal for Nonlinear Mechanics,* vol. 40, pp. 729-46, 2005.

[15] M. Peeters, Viguie, R., Serandour, G., Kerschen, G., and Golinval, J.C., "Nonlinear Normal Modes, Part II: Toward a Practical Computation using Numerical Continuation Techniques," *Mechanical Systems and Signal Processing,* vol. 23, pp. 195-216, 2009.

[16] S. A. Neild, Cammarano, A., and Wagg, D.J.,, "Towards a Technique for Nonlinear Modal Analysis," in *ASME International Design Engineering Technical Conferences and Computers and Information in Engineering Conference*, 2012.

[17] H. Ardeh and M. Allen, "Investigating Cases of Jump Phenomenon in a Nonlinear Oscillatory System," in *Topics in Nonlinear Dynamics, Volume 1*. vol. 35, G. Kerschen, D. Adams, and A. Carrella, Eds., ed: Springer New York, 2013, pp. 299-318.

[18] R. J. Kuether, and Allen, M.S., "A numerical approach to directly compute nonlinear normal modes of geometrically nonlinear finite element models," *Mechanical Systems and Signal Processing,* vol. 46, pp. 1-15, 2014.

[19] R. J. Kuether, and Allen, M.S., "Computing Nonlinear Normal Modes Using Numerical Continuation and Force Appropriation," presented at the 24th Conference on Mechanical Vibration and Noise, 2012.

[20] R. J. Kuether, B. Deaner, M. S. Allen, and J. J. Hollkamp, "Evaluation of Geometrically Nonlinear Reduced Order Models with Nonlinear Normal Modes," *AIAA Journal,* vol. Submitted August, 2014.

[21] T. P. Sapsis, D. D. Quinn, A. F. Vakakis, and L. A. Bergman, "Effective stiffening and damping enhancement of structures with strongly nonlinear local attachments," *Journal of Vibration and Acoustics, Transactions of the ASME,* vol. 134, 2012.

[22] M. Peeters, G. Kerschen, and J. C. Golinval, "Dynamic testing of nonlinear vibrating structures using nonlinear normal modes," *Journal of Sound and Vibration,* vol. 330, pp. 486-509, 2011.
[23] M. Peeters, G. Kerschen, and J. C. Golinval, "Modal testing of nonlinear vibrating structures based on nonlinear normal modes: Experimental demonstration," *Mechanical Systems and Signal Processing,* vol. 25, pp. 1227-1247, 2011.
[24] M. Peeters, G. Kerschen, J. C. Golinval, C. Stéphan, and P. Lubrina, "Nonlinear Normal Modes of a Full-Scale Aircraft," in *Modal Analysis Topics, Volume 3*, T. Proulx, Ed., ed: Springer New York, 2011, pp. 223-242.
[25] G. Kerschen, K. Worden, A. F. Vakakis, and J.-C. Golinval, "Past, present and future of nonlinear system identification in structural dynamics," *Mechanical Systems and Signal Processing,* vol. 20, pp. 505-592, 2006.
[26] J. P. Noel, Renson, L., Grappasonni, C., and Kerschen, G., "A Rigorous Phase Separation Method for Testing Nonlinear Structures," in *Proceedings of ISMA International Conference on Noise and Vibration Engineering*, 2014.
[27] D. Goge, Boswald, M., Fullekrug, U., and Lubrina, P.,, "Ground Vibration Testing of Large Aircraft - State of the Art and Future Perspectives," presented at the XXV International Modal Analysis Conference, Orlando, FL, 2011.
[28] B. Peeters, Climent, H., de Diego, R., de Alba, J., Rodriques Ahlquist, J., Martinez Carreno, J., Hendricx W., Rega, A., Garcia, G., Deweer, J., and Debille, J.,, "Modern Solutions for Ground Vibration Testing of Large Aircraft," presented at the XXVI International Modal Analysis Conference, Orlando, FL, 2008.
[29] P. Lubrina, Giclais, S., Stephan, C., Boeswald, Y., Govers, DLR., "Airbus A350 XWB GVT: State of the art Techniques to Perform a Faster and Better GVT Campaign," in *International Modal Analysis Conference XXXII*, Orlando, FL, 2014.
[30] R. C. Lewis, and Wrisley, D.L., "A System for the Excitation of Pure Natural Modes of Complex Structure," *Journal of the Aeronautical Sciences (Institute of the Aeronautical Sciences),* vol. 17, pp. 705-722, 1950/11/01 1950.
[31] B. Fraeijs de Veubeke, *A variational approach to pure mode excitation based on characteristic phase lag theory*. Paris, France: North Atlantic Treaty Organization, Advisory Group for Aerospace Research and Development, 1956.
[32] D. Otte, Van der Auweraer, H., Debille, J., and Leuridan, J., "Enhanced Force Vector Appropriation Methods for Normal Mode Testing," in *Preeceedings of the 17th International Seminar on Modal Analysis*, 1992.
[33] J. R. Wright, Cooper, J.E., and Desforges, M.J., "Normal Mode Force Appropriation - Theory and Application," *Mechanical Systems and Signal Processing,* vol. 13, pp. 217-240, 1999.
[34] P. A. Atkins, Wright, J.R., and Worden, K., "An Extension of Force Appropriation to the Identification of Nonlinear Multi Degree of Freedom Systems," *Journal of Sound and Vibration,* vol. 237, pp. 23-43, 2000.
[35] A. A. Muravyov, and Rizzi, S.A., "Determination of Nonlinear Stiffness with Application to Random Vibration of Geometrically Nonlinear Structures," *Computers and Structures,* vol. 81, pp. 1513-1523, 2003.
[36] R. W. Gordon and J. J. Hollkamp, "Reduced-order Models for Acoustic Response Prediction," Air Force Research Laboratory, AFRL-RB-WP-TR-2011-3040, Dayton, OH2011.
[37] J. J. Hollkamp and R. W. Gordon, "Reduced-order models for nonlinear response prediction: Implicit condensation and expansion," *Journal of Sound and Vibration,* vol. 318, pp. 1139-1153, 2008.
[38] T. L. Hill, Cammarano, A., Neild, S.A., and Wagg, D.J., "Interpreting the Forced Response of a Two-Degree-of-Freedom Nonlinear Oscillator using Backbone Curves," *Journal of Sound and Vibration,* vol. 349, pp. 276-288, 2015.
[39] R. J. Kuether, Renson, L., Detroux, T., Grappasonni, C., Kerschen, G, and Allen, M.S., "Nonlinear Normal Modes, Modal Interactions, and Isolated Resonance Curves," *Mechanical Systems and Signal Processing,* vol. 351, pp. 299-310, 2015.
[40] M. I. McEwan, Wright, J.R., Cooper, J.E., and Leung, A.Y.T., "A Combined Modal/Finite Element Analysis Technique for the Dynamic Response of a Nonlinear Beam to Harmonic Excitation," *Journal of Sound and Vibration,* vol. 243, pp. 601-624, 2001.

[41] S. W. Shaw, "An Invariant Manifold Approach to Nonlinear Normal Modes of Oscillation," *Journal of Nonlinear Science,* vol. 4, pp. 419-448, 1994.
[42] C. Torrence, and Compo, G.P., "A Practical Guide to Wavelet Analysis," *Bulletin of the American Meteorological Society,* vol. 79, 1998.
[43] M. Feldman, "Hilbert Transform in Vibration Analysis," *Mechanical Systems and Signal Processing,* vol. 25, pp. 735-802, 2011.
[44] M. Kurt, "Identificatoin, Reduced Order Modeling, and Model Updating of Nonlinear Mechanical Systems," PhD, Mechanical Engineering, University of Illinois at Urbana-Champaign, Urbana, Illinois, 2014.
[45] R. W. Gordon, Hollkamp, J.J., and Spottswood, S. M., "Non-linear Response of a Clamped-Clamped Beam to Random Base Excitation," presented at the VIII International Conference on Recent Advances in Structural Dynamics, Southampton, United Kingdom, 2003.
[46] D. A. Ehrhardt, Allen, M.S., Yang, S., and Beberniss, T.J.,, "Full-Field Linear and Nonlinear Measurements using Continuous-Scan Laser Doppler Vibrometry and High Speed Three-Dimensional Digital Image Correlation," *Mechanical Systems and Signal Processing,* vol. In Review, 2015.
[47] S. Yang, and Allen, M.S., "Output-Only Modal Analysis Using Continuous-Scan Laser Doppler Vibrometry and Application to a 20kW Wind Turbine," *Mechanical Systems and Signal Processing,* vol. 31, August 2012 2011.
[48] D. A. Ehrhardt, Yang, S., Beberniss, T.J., and Allen, M.S., "Mode Shape Comparison Using Continuous-Scan Laser Doppler Vibrometry and High Speed 3D Digital Image Correlation," presented at the International Modal Analysis Conference XXXII, Orlando, FL, 2014.
[49] D. A. Ehrhardt, "A Full-Field Experimental and Numerical Investigation of Nonlinear Normal Modes in Geometrically Nonlinear Structures," PhD, Engineering Mechanics, University of Wisconsin-Madison, 2015.
[50] K. Alexiou, and Wright, J.R., "Comparison of MultiPoint Vibration Test Methods," presented at the IX International Modal Analysis Conference, Florence, Italy, 1991.
[51] M. Geradin, and Rixen, D., *Mechanical Vibrations; Theory and Application to Structural Dynamics*: Wiley, 1997.
[52] E. J. Breitbach, "A Semi-Automatic Modal Survey Test Technique for Complex Aircraft and Spacecraft Structures," in *Proceedings of 3rd ESA Testing Symposium*, 1973, pp. 519-528.

5.1 Linear Normal Modes

5.1.1 Introduction

Linear Normal Modes (LMNs) have become fundamental to the understanding of linear dynamics and are rooted in the conservative free vibration equations of motion (EOM), which can be written as follows for a *n* degree of freedom (DOF) system:

$$\mathbf{M}\ddot{\mathbf{x}}(t) + \mathbf{K}\mathbf{x}(t) = 0 \tag{12}$$

where $\mathbf{M}$ is the n x n mass matrix, $\mathbf{K}$ is the n x n stiffness matrix, $\mathbf{x}(t)$ is an n x 1 vector of the displacement of the system, and $\ddot{\mathbf{x}}(t)$ is an n x 1 vector of the acceleration. Using the method of undetermined coefficients, the acceleration and displacement of the system can be represented in the exponential form:

$$\ddot{\mathbf{x}}(t) = \mathrm{Re}\left(-\omega^2 \mathbf{X} e^{i\omega t}\right); \qquad \mathbf{x}(t) = \mathrm{Re}\left(\mathbf{X} e^{i\omega t}\right) \tag{13}$$

where $\mathbf{X}$ is a vector of real variables and ω is the excitation frequency. By substituting Eqn. **Error! Reference source not found.** into Eqn. **Error! Reference source not found.** and rearranging, one obtains the familiar eigenvalue problem:

$$\left(\mathbf{K} - \omega^2 \mathbf{M}\right)\mathbf{X} = 0 \tag{14}$$

5.1.2 Review of Linear Normal Mode Measurement with Force Appropriation

As mentioned previously, phase resonance testing is a method whereby a harmonic force is applied to the structure and then tuned through force appropriation until the mode has been isolated. Tuning methods can be split be split into iterative and direct methods [33, 50], but all methods find roots in the characteristic phase lag theory [31].

Beginning with an N degree of freedom (DOF) system, the forced response of a system can be represented by:

$$\mathbf{M}\ddot{\mathbf{x}}(t) + \mathbf{K}\mathbf{x}(t) + \mathbf{f}_{\mathbf{d}} = \mathbf{f}_{\mathbf{in}}(t) \tag{15}$$

Where $\mathbf{M}$ is the mass matrix, $\mathbf{K}$ is the stiffness matrix, and $\mathbf{f}_{\mathbf{d}}$ are the damping forces, which may come from linear viscous damping or linear material damping and hence may be dependent on displacement or velocity. $\mathbf{f}_{\mathbf{in}}(t)$ is the input force vector, which can be assumed to take the form:

$$\mathbf{f}_{\mathbf{in}}(t) = \mathrm{Re}\left(\mathbf{F}e^{\mathrm{i}\omega t}\right) \tag{16}$$

Where $\mathbf{X}$ and $\mathbf{F}$ and are vectors of real variables, ω is the excitation frequency. If the structure has classical, undamped modes, then the response can be written as $\mathbf{x}(t) = \mathrm{Re}(\mathbf{X}e^{i\omega t-\theta})$, where θ is the phase lag of the response relative to the force. There are several forms $\mathbf{f}_{\mathbf{d}}$ can take depending on the dissipation characteristics expected in the structure investigated. Two common forms of linear damping are viscous and structural, which have the following form for harmonic motion:

$$\mathbf{f}_{\mathbf{d}} = \mathrm{Re}\left(i\omega\mathbf{C}\mathbf{X}e^{i(\omega t-\theta)} + i\mathbf{D}\mathbf{X}e^{i(\omega t-\theta)}\right) \tag{17}$$

Where $i\omega\mathbf{C}$ is related to linear viscous damping and $i\mathbf{D}$ is related to structural damping (e.g. $\mathbf{D}=\eta\mathbf{K}$ where η is the material loss factor), and both are 90 degrees out of phase from the response due the i term in each expression. As a result, both are in phase with the structure's velocity. Using the definitions established in Eqns. (16) and **Error! Reference source not found.**, and pulling out the coefficients of the damping terms, Eqn. **Error! Reference source not found.** can be separated into imaginary and real parts with the phase in the complex exponential separated into sine and cosine terms.

$$\left[\left(\mathbf{K} - \omega^2\mathbf{M}\right)\sin\theta - \mathbf{F}_{\mathbf{d}}\cos\theta\right]\mathbf{X} = 0 \tag{18}$$

$$\left[\left(\mathbf{K} - \omega^2\mathbf{M}\right)\cos\theta + \mathbf{F}_{\mathbf{d}}\sin\theta\right]\mathbf{X} = \mathbf{P} \tag{19}$$

As discussed by de Veubeke [31], when the response has a delay of 90 degrees with the input force vector, Eqn. **Error! Reference source not found.** only contains the relationship between the stiffness and mass of the structure and Eqn. **Error! Reference source not found.** only contains the effect from damping, which is balanced by the input force vector. For this phase criterion, the excitation frequency is at the undamped natural frequency of the structure, $\omega = \omega_n$, and the mono-phased response displacement, $\mathbf{X}$, is the *Normal Mode* shape.

Before proceeding to discuss nonlinear systems, it is beneficial to examine the force that must be applied to isolate a linear mode using the energy balancing technique [38, 39, 51]. This technique provides an approximate description of the input forced needed to cancel the damping in the structure; however, for a perfect force appropriation the energy would have to be equal at all times. For the purposes of this investigation, the average is assumed to be sufficient in the appropriation of a normal mode. If the system is oscillating on a LNM, the power dissipated at any instant is:

$$\mathbf{P}_{diss} = \dot{\mathbf{x}}(t)^{\mathrm{T}}\mathbf{C}\dot{\mathbf{x}}(t) \tag{20}$$

Where only the viscous damping case has been considered for simplicity. The total energy dissipated over one period of the response is:

$$E_{diss/cyc} = \int_0^T \mathbf{P}_{diss} dt = \int_0^T \dot{\mathbf{x}}(t)^{\mathrm{T}} \mathbf{C} \dot{\mathbf{x}}(t) dt \tag{21}$$

Similarly, for a forcing function $\mathbf{f_{in}}(t)$, the energy the external force inputs into the system is:

$$E_{in/cyc} = \int_0^T \dot{\mathbf{x}}(t)^{\mathrm{T}} \mathbf{f_{in}}(t) dt \tag{22}$$

At resonance the energy dissipated by the damping forces must equal the total energy input to the system over the period T:

$$E_{diss/cyc} = E_{in/cyc} \tag{23}$$

and by equating these two expressions one can determine what force to exert to isolate a known mode, $\mathbf{X}$, at a given amplitude.

For a structure with well separated modes, a single-point mono-harmonic force is all that is needed to isolate a LNM. Note that such a force is not necessarily a good approximation to the dissipative forces in the structure, but this works because the total energy input per cycle matches the energy dissipated and the energy absorbed by modes other than the mode of interest ends up being very small. In this context, when a single-point, mono-harmonic force $f_{in}(t)=A\sin(\omega t)$ is applied at a location n on the structure, with amplitude A, the energy balance criterion in the equation above becomes:

$$\int_0^T \dot{\mathbf{x}}(t)^{\mathrm{T}} \mathbf{C} \dot{\mathbf{x}}(t) dt = A \int_0^T \dot{x}_n(t) \sin(\omega t) dt \tag{24}$$

where $\dot{x}_n$ denotes the velocity of the structure at the point where the force is applied.

This energy balance criterion provides a direct link between the computed LNMs and the resonant response of the damped forced system [39]. If the response is not 90 degrees out of phase with the force, then over the course of a cycle the input forces alternately add and remove energy from the system and the motion, $\mathbf{x}(t)$, that is measured is not an invariant of the structure but depends on the forcing.

In an experiment, the mode is not known a priori so an in situ "hard tuning" of each mode is used to bring the isolated mode to some specified level of accuracy. An overview and comparison of different force appropriation methods can be found in [33]. The response can be fit to a complex model, $\mathbf{x}(t) = \mathrm{Re}(\mathbf{Z}e^{i\omega t})$, where $\mathbf{Z}$ is the complex amplitude of the response and the following modal indicator function can be checked to determine how close the measured response is to a pure normal mode [33, 52]:

$$\Delta = \frac{\mathrm{Re}\{\mathbf{X}\}^{\mathrm{T}} \mathrm{Re}\{\mathbf{X}\}}{\mathbf{X}^{\mathrm{H}} \mathbf{X}} \tag{25}$$

where $()^{\mathrm{H}}$ is the Hermitian.